UNIVERSITA' VITA-SALUTE SAN RAFFAELE

CORSO DI DOTTORATO DI RICERCA

IN MEDICINA MOLECOLARE
Curriculum in Neuroscienze e Neurologia Sperimentale

INVESTIGATING THE NON-CELL AUTONOMOUS EFFECTS OF THE TDP-43 P.A382T MUTATION IN SCHWANN CELLS USING AN IN VIVO AND AN IN VITRO MODEL

Supervisore: dott. Angelo Quattrini

Co-supervisore: prof. Pietro Fratta

Tesi di DOTTORATO di RICERCA di Tommaso Russo matr. 022772
Ciclo di dottorato XXXVIII
SSD MED/26

Anno Accademico 2024/2025

CONSULTAZIONE TESI DI DOTTORATO DI RICERCA

Il/la sottoscritto Tommaso Russo

Matricola 022772
nato a Roma.
il 14/05/1993

autore della Tesi di Dottorato di Ricerca dal titolo

Investigating the non-cell autonomous effects of the TDP-43 p.A382T mutation in Schwann cells using an in vivo and an in vitro model

AUTORIZZA la Consultazione della Tesi

Data 27/11/2025 *Firma*

DECLARATION

This thesis has been:

- composed by myself and has not been used in any previous application for a degree. Throughout the text I use both 'I' and 'We' interchangeably.

- has been written according to the editing guidelines approved by the University.

All the results presented here were obtained by myself, except for:

1) *The generation of the mouse model, including cloning, mutagenesis and verification of transgene expression (Results, chapter "Generation of the in vivo model" was performed by Francesca Florio (Biology of Myelin Unit, Division of Genetics and Cell Biology, IRCCS San Raffaele Scientific Institute) in collaboration with Core Facility for Conditional Mutagenesis (CFCM, IRCCS San Raffaele Scientific Institute).*
2) *Neurophysiological tests (Results, chapter "P0-Cre/hTDP-43 p.A382T mice do not develop any neurophysiological phenotype") were performed by Francesco Gentile (Biology of Myelin Unit, Division of Genetics and Cell Biology, IRCCS San Raffaela Scientific Institute), Serena Valenzano, Silvia Sicardi and Ubaldo Del Carro (Neurophysiology Unit, IRCCS San Raffaele Scientific Institute).*
3) *Analysis of electron microscopy samples (Results, chapter "P0-Cre/hTDP-43 p.A382T mice develop mild neuropathological abnormalities by 9 months of age") was performed by Angelo Quattrini (Experimental Neuropathology Unit, Division of Neuroscience, IRCCS San Raffaele Scientific Institute)*
4) *RTq-PCRs in P0-Cre/hTDP-43 mice (Results, chapter "Molecular characterization of P0-Cre/hTDP-43 p.A382T mice") were performed by Francesca Florio and Roberta De Blasis (Biology of Myelin Unit, Division of Genetics and Cell Biology, IRCCS San Raffaele Scientific Institute).*
5) *The in vitro co-culture model (Results, chapter "In vitro model") was generated and analyzed by Alessandro Romano (Division of Neuroscience, IRCCS San Raffaele, Scientific Institute in Lecce).*
6) *The RT-qPCR in iPSC-derived motor neurons with C9orf72 expansion (Results, chapter "In vitro model") was performed by Ana Rita Agra de Almeida Quadros (Department of Neurology, The Sean M. Healey and AMG Center for ALS, Massachusetts General Hospital, Harvard Medical School)*

All sources of information are acknowledged by means of reference.

ACKNOWLEDGMENTS

I am deeply grateful to Dr. Angelo Quattrini and Dr. Maurizio D'Antonio for their constant support and feedback. I sincerely thank all the people who helped with the experiments, including: Laura Pozzi for her help and supervision in performing molecular biology experiments; Francesca Florio, Roberta De Blasis and Francesco Gentile for their help and supervision in performing mouse behavioral tests and dissections; Giorgia Dina for her help and supervision in performing immunostainings; Clotilde Lagier-Tourenne and Xin Jiang for their mentoring and supervision with the generation and analyses of iPSC-derived motor neurons.

Abstract (English version)

The neuropathological hallmark of amyotrophic lateral sclerosis (ALS), a neurodegenerative disease characterized by the involvement of upper and lower motor neurons, is the presence of mislocalization, aggregation and phosphorylation of the RNA-binding protein TDP-43, referred to as TDP-43 pathology, in affected tissues. In some cases, mutations in TDP-43 are found in patients with ALS, suggesting that TDP-43 has a causative role in the disease. The missense p.A382T variant is the most common in the Italian population of patients with ALS. TDP-43 pathology does not involve only neuronal cells and has been observed in glial cells. Phosphorylated TDP-43 has been observed in both axons and Schwann cells in motor nerve biopsies from patients with ALS in previous studies. In the present project, we tried to evaluate if the expression of TDP-43 with the p.A382T mutation in Schwann cells has a non-cell autonomous role on motor neuron disease.

We generated an iPSC-derived in vitro model, and an in vivo transgenic mouse model.

The in vitro model showed that iPSC-derived Schwann cells from patients with ALS with the TDP-43 p.A382T mutation are toxic to iPSC-derived motor neurons from healthy TDP-WT controls, impairing axonal sprouting.

The in vivo model did not exhibit overt behavioral or neurophysiological phenotypes, probably due to the low-level expression of the transgenic protein. However, adult-onset sporadic neuropathological abnormalities and TDP-43 mislocalization were observed.

In conclusion, our results suggest that the expression of TDP-43 with the p.A382T mutation in Schwann cells might have a non-cell autonomous role and affect motor neuron disease.

Abstract (versione italiana)

Il tratto neuropatologico distintivo della sclerosi laterale amiotrofica (SLA), una malattia neurodegenerativa caratterizzata dal coinvolgimento di primo e secondo motoneurone, è la mislocalizzazione, aggregazione e fosforilazione della proteina TDP-43, nota come patologia da TDP-43, nei tessuti affetti. In alcuni casi, nei pazienti con SLA vengono identificate mutazioni in TDP-43, suggerendo che questa proteina abbia un ruolo causale nella malattia. La variante missenso p.A382T è la più comune mutazione di TDP-43 nella popolazione italiana di pazienti con SLA. La patologia da TDP-43 non riguarda solo le cellule neuronali, ma è stata osservata anche nelle cellule gliali. Studi precedenti hanno riscontrato TDP-43 fosforilata sia negli assoni che nelle cellule di Schwann in biopsie di nervi motori di pazienti con SLA. Nel presente progetto, abbiamo cercato di valutare se l'espressione di TDP-43 con la mutazione p.A382T nelle cellule di Schwann abbia un ruolo nella malattia dei motoneuroni.

Abbiamo generato un modello in vitro derivato da iPSC e un modello murino transgenico in vivo.
Il modello in vitro ha mostrato che le cellule di Schwann derivate da iPSC di pazienti con SLA con mutazione TDP-43 p.A382T sono tossiche per i motoneuroni derivati da iPSC di controlli sani con TDP-WT, compromettendo la crescita degli assoni.
Il modello in vivo non ha mostrato fenotipi comportamentali o neurofisiologici evidenti, probabilmente a causa del basso livello di espressione della proteina transgenica. Tuttavia, sono state osservate anomalie neuropatologiche sporadiche a esordio adulto e mislocalizzazione di TDP-43.

In conclusione, i nostri risultati suggeriscono che l'espressione di TDP-43 con la mutazione p.A382T nelle cellule di Schwann potrebbe avere un ruolo non autonomo e influenzare la malattia dei motoneuroni

Summary

Introduction

Amyotrophic lateral sclerosis: an overview

Amyotrophic lateral sclerosis (ALS) is a neurodegenerative disease, characterized by the progressive degeneration of upper motor neurons (UMNs) and lower motor neurons (LMNs) (Brown & Al-Chalabi, 2017). In ALS, the degeneration of UMNs and LMNs results in the progressive paralysis of skeletal muscles, including those needed for swallowing and breathing. For this reason, ALS ultimately leads to death, usually by respiratory failure, usually in the span of few years after onset, and there is no available treatment capable of stopping disease progression (Hardiman *et al*, 2017).

ALS incidence is about 4 cases out of 100.000 person per year, and changes remarkably among age groups. Despite being considered a rare disease, ALS is a relatively frequent diagnosis in 50- to 70-year-old persons, and the lifetime risk of developing ALS is about 1 to 300 (Feldman *et al*, 2022). Patients of male and female sex assigned at birth can both be involved in a comparable frequency, even though a slight significant risk imbalance towards the male sex is a well-recognized epidemiological finding (Talbott *et al*, 2016). The risk of developing ALS is present throughout the globe. In about 90% of the cases, the disease is sporadic, meaning that the family history is negative for ALS cases, whereas familial ALS accounts for about 10% of cases (Mejzini *et al*, 2019).

ALS is considered a multifactorial disease, and its etiopathogenesis is largely unknown. Disease-associated genetic variants are found in about 10-15% patients, whereas a larger percentage of patients carries variants of uncertain significance in ALS-associated genes (Ruf *et al*, 2023). This percentage is significantly higher in patients with familial forms of ALS. Twin studies suggest that ALS risk is only partially inheritable, supporting the role of currently unknown environmental factors (Al-Chalabi *et al*, 2010). Many progresses have been achieved in the last 20 years for what concerns the genetic factors. The first ALS-associate gene, SOD1 was discovered in 1993 (Rosen *et al*, 1993);

variants in more than 30 genes have been identified as associated to ALS or affecting disease features to date (Mathis *et al*, 2019). Many of these genes encode for proteins involved in specific pathways, including RNA metabolism (e.g. TARDBP, FUS, HNRNPA1), autophagy (e.g. TBK1, OPTN) and axonal transport and structure (e.g. DYNC1H1, DCTN1, NEFH) (Nijs & Van Damme, 2024). The most frequent ALS-associated variant in the Western world is the expansion of an intronic hexanucleotide sequence in the C9ORF72 gene (Renton *et al*, 2011). The discovery of the association between ALS and variants in the TARDBP gene, encoding for the TDP-43 protein, has been of remarkable importance, since inclusions containing this protein are considered the neuropathological hallmark of the disease, thus linking neuropathological evidence to a causal genetic factor (Kwiatkowski *et al*, 2009; Neumann *et al*, 2006).

The presence of intracellular inclusions positive for the TDP-43 protein in ALS affected tissues is the neuropathological hallmark of ALS, reported in >90% of cases, including most sporadic ALS cases. ALS associated with mutations in the SOD1 and in the FUS gene represent exceptions, since they do not show this feature (Mackenzie *et al*, 2007; Feldman *et al*, 2022). TDP-43 is an ubiquitary RNA-binding protein, mostly located in the cell nucleus, which regulates the expression of thousands of genes (Duan *et al*, 2022). In ALS affected tissues, the presence of cytoplasmic TDP-43 positive inclusions is typically accompanied by the loss of nuclear TDP-43 signal (Mackenzie *et al*, 2007). Both TDP-43 loss and gain of function mechanism are thought to play a role in the molecular pathogenesis (de Boer *et al*, 2020).

The most striking gross neuroanatomical finding in ALS is the degeneration of motor neurons and corticospinal tracts ("lateral sclerosis", since the corticospinal tracts run in the lateral part of the spinal cord) (Mead *et al*, 2023). However, the involvement of different neuroanatomical areas and systems is now well-recognized. A high percentage of ALS cases displays cognitive impairment and/or behavioral alterations, which in 10-15% cases consist in overt cases of frontotemporal dementia (FTD) (Strong *et al*, 2017). ALS and FTD do not only frequently overlap; they share genetic and neuropathological features, including TDP-43 pathology in a relevant percentage of cases (Seelaar *et al*, 2007; Abramzon *et al*, 2020). Pathological involvement of the hypothalamus has been also demonstrated, and recently sleep alterations have been observed in pre-symptomatic patients with ALS (Chang *et al*, 2025; Guillot *et al*, 2025). Alterations have been reported also in sensory nerve fibers innervating the skin (Nolano *et al*, 2024).

ALS is a clinically heterogeneous syndrome; the variability regards many features, such as the severity of upper versus lower motor neuron involvement, the selective or widespread anatomical spreading, the site of onset, the age at onset, the prognosis, the presence of cognitive impairment (van Es *et al*, 2017). Some of these features can be thought as spectra; for example, lower motor

involvement can be extremely prominent in pure lower motor neuron syndromes, where upper motor neuron involvement can be virtually undetectable (Schito *et al*, 2020).

An unsolved question regards ALS spreading. Some evidence suggests the view that pathological changes in ALS starts in the brain and then spreads in a corticofugal pattern (Braak *et al*, 2013). On the other hand, the peripheral nerve and especially the neuromuscular junctions are apparently affected at a very early timepoint (Fischer *et al*, 2004).

In synthesis, ALS is a complex multifactorial disease, which despite its heterogeneity shares a common molecular pathology; it is not limited to the motor neurons, and the disease spreading pattern is still unclear.

Anatomy of the peripheral nerve

The microscopic anatomy of the peripheral nerve is composed by different structural and cellular components. The epineurium is the outermost part of the peripheral nerve, composed by connective tissue organized in collagen bundles which run longitudinally along the perineurium. The epineurium has its own vascularization and lymphatic drainage system (Stewart, 2003). The perineurium is a structure formed by one or more layers of perineurial cells, which surrounds each nerve fascicle. It represents a continuum with the leptomeningeal layer from the central nervous system and extends distally to ensheath peripheral sensorial organs (Piña-Oviedo & Ortiz-Hidalgo, 2008). Perineurial cells have their own basement membrane, are connected by tight junctions and express the transporter Glut1, suggesting a barrier function (blood-nerve barrier) (Malong *et al*, 2023). The perineurial tight junctions express claudin 1 and 3, occluding and Zo-1 (Iwanaga *et al*, 2022). Perineurial cells are likely involved in the trafficking of molecules inwards and outwards the nerve fascicles, as suggested by the active pinocytosis observed in ultrastructural imaging (Peltonen *et al*, 2013). The barrier function of the perineurium is also important in neoplastic processes, and perineurial invasion is a negative prognostic factor in cancer (Piña-Oviedo & Ortiz-Hidalgo, 2008). After nerve damage, the perineurium can regenerate from differentiation of resident endoneurial fibroblasts (Hirasawa *et al*, 1994). The endoneurium is the region internal to the perineurium, which contain the axon-Schwann cell units in an extracellular matrix. The endothelial cells of the endoneurial vessels, endoneurial pericytes, their basement membrane, as well as macrophages and support cells known as tactocytes, participate to the blood-nerve barrier at the endoneurial level (Malong *et al*, 2023).

The nerve fascicles include both myelinated and non-myelinated axons. Myelinated axons are larger than unmyelinated ones (Salzer, 2015). Each segment of a myelinated fiber is associated to a single Schwann cell. Every segment defines an internode, usually long from 200 to 1800 um (Salzer, 2015). The short (~1 um) region of a myelinated fiber not surrounded by myelin is the node of Ranvier,

whereas the specialized border region between mode and internode is referred to as paranode (Schumacher *et al*, 2025). The paranodal axoglial junction physically connects the myelin sheath to the axon at the end of each internodal segment. This structure keeps segregation between axolemmal districts, since the membrane protein milieu of the node of Ranvier is highly specific and channel clustering is necessary for efficient nerve conduction (Fehmi *et al*, 2018). The thickness of the myelin sheath is proportional to the axonal diameter, and the ratio between the naked axon diameter and the fully myelinated axon diameter ranges between 0.5 and 0.7 (G-ratio) (Jessen *et al*, 2015).

Unmyelinated nerve fibers are spread in the nerve fascicle and are usually more abundant than myelinated ones. These axons are associated with non-myelinating Schwann cells, which can interact with more than one fiber (Remak bundles) (Jessen *et al*, 2015).

The role of Schwann cells

Schwann cells (SCs) are key support glial cells in the peripheral nervous system. SCs derive embryologically from the neural crest, first developing in pluripotent SC precursors and then into immature SCs, which can differentiate into myelinating SCs or nonmyelinating SCs (Remak) (Wilson *et al*, 2021). A specific nonmyelinating SC subtype is the perisynaptic SC, which surrounds the motor axon terminal at the neuromuscular junction and actively participate in the synapse formation (Jessen *et al*, 2015). These perisynaptic SCs are also important in axonal regeneration after damage. When motor fibers are injured, surviving fibers sprout their axons to reinnervate denervated motor end plates, a process promoted by perisynaptic SCs (Gould *et al*, 2025; Son & Thompson, 1995).

In early embryonic development, proliferating SC precursors reach to developing peripheral nerves and differentiate in immature SCs (iSCs), under the control of the transcription factor Sox10 (Feltri *et al*, 2016). Groups of immature SCs surround bundles of axons and start to depose their basal lamina around them. Then, iSCs actively select larger caliber axons by protruding their processes and segregating those axons to the periphery of the bundle, a process called radial sorting (Wilson *et al*, 2021). These larger axons will be then myelinated by a myelinating SC which interacts only with one axon. In the meanwhile, iSCs also play a major role in the formation of nerve vasculature, perineurium and epineurium. The myelination is chemically driven by the exposure of neuregulin I type III on the axonal membrane, which is also necessary for the survival and differentiation fate of SC precursors (Taveggia *et al*, 2005). The pro-myelinating SCs switch to express high levels of myelin-associated proteins such as P0, MBP and PMP22, along with the enzymes needed for lipid biosynthesis, under the control of the transcriptional regulator Krox20 (Topilko *et al*, 1994). The rest of the smaller axons instead are wrapped by the cytoplasm of nonmyelinating SCs, an interaction necessary for axonal survival. Thus, SCs are important to guide the arrangement of the peripheral nerve during

development. The myelination process in the peripheral nervous system starts perinatally and continues in the early postnatal phase in vertebrates. SCs are also necessary for axonal survival during development, likely by providing pro-survival signaling and ensuring correct target reaching for motor axons (Wiedemann, 2010; Feltri *et al*, 2016). SCs have their own basal lamina, which includes specific laminins required for normal radial sorting; the basal lamina is linked to the SC membrane by integrins and dystroglicans (Ghidinelli *et al*, 2017). The SC differentiation process is reversible, and SCs can de-differentiate upon injury during the process of nerve repair and regeneration (Jessen & Mirsky, 2016).

The myelin sheath provided by mature myelinating SCs is necessary for an effective nerve conduction along the peripheral nerve. Myelin is a multilamellated tightly compacted substance produced from the Schwann cell plasma membrane that wraps and insulates the axons. It is mainly composed by lipids (phospholipids, glycolipids, and cholesterol) and proteins, including myelin glycoproteins P0, P1 and P2, PMP-22 and MAG, to cite the most relevant ones(Scherer & Wrabetz, 2008). P0 is the most abundant one, and it is specific of the peripheral nervous system (Greenfield *et al*, 1973).

The myelin sheath interacts with the axolemma at the paranodal junctions. The paranode compartmentalizes the node of Ranvier from the rest of the axon. The junction relies on the binding of myelinic neurofascin 155 with axonal contactin-1 and contactin-associated protein (CASPR). At the level of the node, SCs project extroflections known as microvilli and take contact with the axolemma via the interaction of gliomedin with axonal neurofascin 186 (Rasband & Peles, 2016).

The pathophysiology of many genetic and acquired conditions involves a damage or an incorrect formation of the myelin sheath, resulting in slow conduction velocity at the neurophysiological examination and to the presence of sensitive and motor dysfunction at the clinical examination (Fridman & Saporta, 2021). Interestingly, it is frequent to observe the concomitance of axonal damage, especially in long-standing demyelinating or hypomyelinating diseases, underlining the importance of myelination and SC support for the nerve fibers (Moss *et al*, 2021).

Myelination of axons can be replicated in vitro by using primary rat SCs (Negro *et al*, 2022). Human SCs, either primary or induced form other cell-types, cannot myelinate axons in vitro (Hörner *et al*, 2022). Direct differentiation of human skin fibroblasts into SCs can be induced by transgenic overexpression of key transcriptional regulator Sox10 and Krox20 (Mazzara *et al*, 2017); human pluripotent stem cells can be induced into SCs by exposure to molecules such as neuregulin, forskolin, and ascorbic acid (Kim *et al*, 2017).

TDP-43: physiology and pathology

Transactive response DNA-binding protein 43 is a protein encoded by the TARDBP gene, located on chromosome 1. It is expressed in substantially all nucleated cells and evolutionarily highly conserved (Jo *et al*, 2020). The protein structure consists of a N-terminal domain, two RNA recognition motifs (RRM1 and RRM2) and a C-terminal domain (CTD), also known as low complexity domain, with a high content of glycine and amyloid-like properties (Duan *et al*, 2022). These features confer to the CTD an high tendency to aggregate (Scialò *et al*, 2025). TDP-43 subcellular location is mainly nuclear; however, TDP-43 can shuttle inside and outside the nuclear membrane and dynamically transfer to the cytoplasm (Duan *et al*, 2022). TDP-43 can undergo specific post-translational modifications, such as phosphorylation, acetylation, and cleavage, which affect its localization, function and solubility (Buratti, 2018).

TDP-43 ablation is incompatible with life, suggesting a key role in early development (Sephton *et al*, 2010). TDP-43 is involved in RNA processing and splicing, transport, and translation (Jo *et al*, 2020); indeed, TDP-43 was early recognized as a splicing regulator factor for the CFTR gene (Buratti & Baralle, 2001). TDP-43 strictly regulates its own levels, by binding to its own 3'UTR and modulating its own alternative splicing (Ayala *et al*, 2011). As an RNA-binding protein, TDP-43 preferentially binds UG RNA motifs (Tollervey *et al*, 2011). TDP-43 can bind to and regulate the splicing of a large number of mRNAs (Polymenidou *et al*, 2011).

TDP-43 also participates in the formation of stress granules, which are membrane-less organelles consisting of untranslated mRNA and RNA-binding proteins (Colombrita *et al*, 2009). Stress granules assemble by liquid-liquid phase separation upon environmental stress and then disassemble spontaneously (Guillén-Boixet *et al*, 2020). Recent evidence suggest that altered dynamics in stress granule formation might be a trigger for TDP-43 pathological aggregation (Yan *et al*, 2025).

TDP-43 has also been involved in the transport of transcripts along the axon towards the synaptic terminal and in regulating local translation at the neuromuscular junction (Piol *et al*, 2023).

In 2006, TDP-43 was recognized as one of the main components of the ubiquitinated inclusions found in postmortem ALS and FTD affected tissues (Neumann *et al*, 2006). Interestingly, clearing of nuclear TDP-43 was observed in neurons bearing the ubiquitinated inclusions (Mackenzie *et al*, 2007). TDP-43 mislocalization was found to be associated to loss of its splicing regulator function (Yang *et al*, 2014). The mislocalization of the TDP-43 protein from the nucleus to the cytoplasm, where it forms insoluble, hyperphosphorylated, and ubiquitinated aggregates, with disruption of its normal function, is referred to as TDP-43 pathology (de Boer *et al*, 2020). The severity of TDP-43 pathology correlates with neuronal loss and with white and grey matter involvement in ALS (Brettschneider *et al*, 2013). TDP-43 pathology has been reported also as in neurodegenerative diseases other than ALS and FTD,

including Alzheimer disease and Huntington chorea (Nguyen *et al*, 2025; Agra Almeida Quadros *et al*, 2024). Data from different diseases associated to TDP-43 pathology showed that the structure of cytoplasmic TDP-43 inclusions might be connected to the clinical phenotype (Neumann *et al*, 2021; Arseni *et al*, 2023). Importantly, TDP-43 pathology is not exclusive of neurons, and has been observed also in glial cells such as astrocytes (Licht-Murava *et al*, 2023), oligodendrocytes (Lorente Pons *et al*, 2020), and microglia (Boillée *et al*, 2006). Studies from in vitro and in vivo models suggest that TDP-43 dysfunction in glial cells might impact disease progression (Ditsworth *et al*, 2017; Yamanaka *et al*, 2008; Boillée *et al*, 2006).

TDP-43 knockdown in vitro leads to wide alterations at transcriptomic level, including the retention of noncanonical exons ("cryptic" exons), which can cause the generation of premature transcript termination, nonsense mediated decay, or the production of noncanonical peptides (Brown *et al*, 2022). Notably, these transcriptomic alterations are specie-specific, since they rely on the binding of TDP-43 to non-conserved UG rich intronic sequences, and cell-type specific (Ling *et al*, 2015; Šušnjar *et al*, 2022). In 2019, two research groups showed that the splicing dysregulation consequent to TDP-43 knockdown in human neuronal cells, specifically the inclusion of a non-canonical exon in STMN2 transcript causing its truncation, recapitulated those seen in patient-derived cells and postmortem tissues (Melamed *et al*, 2019; Klim *et al*, 2019). STMN2 protein is important for microtubule dynamics and neuromuscular junction integrity, and restoration of STMN2 expression rescues the phenotype in vitro (Melamed *et al*, 2019). Few years later, starting from the observation that a SNP in UNC13A gene was associated with higher ALS and FTD risk and worse prognosis (Chiò *et al*, 2013), it was found that TDP-43 knockdown results in the inclusion of a non-canonical exon in UNC13A transcript, leading to nonsense mediated decay (Brown *et al*, 2022; Ma *et al*, 2022).

Pathological TDP-43 can template its own misfolding and aggregation (Nonaka *et al*, 2013; Laferrière *et al*, 2019), which can then induce its loss of function (Scialò *et al*, 2025). Increasing evidence suggest that TDP-43 pathology might propagate in a prion-like fashion, driving disease spreading (Scialò *et al*, 2025).

It is still unknown whether TDP-43–driven neurodegeneration is caused by loss of its nuclear splicing role, by toxic effects arising in the nucleus or cytoplasm, or, most likely, by a co-occurrence of these factors.

Non-cell autonomous pathogenic mechanisms in ALS

ALS has long been considered a disease primarily driven by intrinsic motor neuron pathology. However, evidence indicates that non-neuronal cells might contribute to disease initiation and progression of ALS. TDP-43 containing aggregates have been observed in oligodendrocyte and

astrocyte cytoplasm in postmortem samples from ALS patients (Neumann *et al*, 2007; Brettschneider *et al*, 2014; Nishihira *et al*, 2008). Astrocytes extracted from fresh postmortem ALS samples are toxic to motor neurons in vitro (Haidet-Phillips *et al*, 2011). Expression of disease-associated TDP-43 in astrocytes triggers neurodegeneration in mouse models (Tong *et al*, 2013), whereas an astrocyte-selective TDP-43 knock-out resulted in motor deficits and astrocytic changes, without motor neuron loss (Peng *et al*, 2020). iPSC-derived astrocytes from ALS patients with a disease-associated TDP-43 mutation show cell autonomous toxicity (Serio *et al*, 2013). Patient-derived oligodendroglia is toxic to motor neurons in vitro (Ferraiuolo *et al*, 2016). TDP-43 knock-out in oligodendrocyte precursors led instead only to cell-autonomous phenotype (Wang *et al*, 2018; Heo *et al*, 2022).

Microglial activation is also observed in ALS postmortem samples (Brettschneider *et al*, 2012), with transcriptomic features showing disease-associated microglia signature (Dols-Icardo *et al*, 2020). Nuclear medicine data support the presence of microglial activation in vivo in patients (Turner *et al*, 2004; Tondo *et al*, 2020). Evidence from mouse models suggests that microglial cells play a protective role for motor neurons (Spiller *et al*, 2018; Xie *et al*, 2022).

The role of Schwann cells, the main glial cells in the peripheral nervous system, in ALS is still unclear. TDP-43 pathology has been observed in SCs from living and post-mortem ALS nerve samples (Riva *et al*, 2022; Nakamura-Shindo *et al*, 2020). Loss of TDP-43 in SCs results in paranodal alterations with decreased conduction velocity in a mouse model (Chang *et al*, 2021).

Peripheral nervous system involvement in ALS

Peripheral nervous system involvement is relatively understudied in ALS research. Its involvement is the most evident disease manifestation in most cases, since muscle atrophy and fasciculations are signs of muscle fiber denervation and motor axon dysfunction, respectively (de Carvalho & Swash, 2023). Phosphorylated TDP-43 inclusions have been reported in the motor axons, not only in the neuronal soma (Kurashige *et al*, 2022; Riva *et al*, 2022). TDP-43 plays a role in the transport of mRNA containing granules along the axon towards the synaptic terminal (Piol *et al*, 2023). Moreover, aggregates positive for pTDP-43 have been reported also in the muscle of postmortem samples from patients with ALS and in living patients with ALS, even prior to clinical or neurophysiological involvement (Cykowski *et al*, 2018; Zhang *et al*, 2024).

The dying-back theory suggests that the distal axon and the neuromuscular junction might be the primary location of degeneration in ALS (Fischer *et al*, 2004). The NMJ denervation phenotype has been reproduced in mouse models of TDP-43 pathology and NMJ functional defects precede the onset of motor impairment in these models (Alhindi *et al*, 2023; Chand *et al*, 2018).

Studies have shown that demyelination and remyelination disturbances are present in nerve biopsies of ALS patients, suggesting SC dysfunction in the disease pathogenesis (Heads *et al*, 1991) and post-mortem studies have demonstrated areas of demyelination together with motor neuron degeneration (Sobue *et al*, 1981; Zhou *et al*, 2017). Myelinating SCs are known to promote repair after nerve injury, but this response might be overwhelmed by the neurodegenerative process in ALS (Martineau *et al*, 2020). In a mouse model of ALS, perisynaptic SC alterations precede motor end plate denervation and that perisynaptic SC pathology leads to sprouting deficits after denervation (Carrasco *et al*, 2016; Harrison & Rafuse, 2020).

In previous research from our group, axonal phosphorylated TDP-43 (pTDP-43) inclusions have been found in the motor nerve of living patients with ALS, with a high sensitivity; these inclusions were not specific of ALS, since they were also found in other neuromuscular diseases (Riva *et al*, 2022). Importantly, motor nerves of patients with ALS showed axonal pTDP-43 positivity also in nerves without signs of axonal degeneration, supporting a pathogenesis model in which TDP-43 pathology precedes neurodegeneration. Interestingly, also Schwann cells displayed pTDP-43 positivity in a relevant percentage of cases (Riva *et al*, 2022).

Mouse models of TDP-43 pathology

Different mouse models of TDP-43 pathology, more than 40 to date, have been developed to mimic the pathological features of ALS or to study the effects of an altered TDP-43 expression on specific cell-types. Some examples include: the constitutive or conditional overexpression of transgenic TDP-43 (mutated or WT); the insertion of a mutation in the endogenous mouse gene; the conditional knock-out of the endogenous gene (Armas *et al*, 2025). The complexity of TDP-43 pathology is difficult to recapitulate entirely in models, and some models exhibit only partial aspects of it (e.g inclusion formation, but not loss of function). However, some of these models exhibit TDP-43 proteinopathy, motor neuron degeneration, and altered splicing, similarly to what is observed in human ALS (Tsai *et al*, 2010; Janssens *et al*, 2013; Arnold *et al*, 2013; Igaz *et al*, 2011; Walker *et al*, 2015; Godoy-Corchuelo *et al*, 2024). Notably, it has been suggested that although TDP-43 overexpression is toxic in models, this toxicity might occur via different pathways to those observed in human disease (Heo *et al*, 2022).

Previous work tried to evaluate the effect of TDP-43 knock-out in glial cells using mouse models, in order to investigate whether TDP-43 dysfunction might exert a non-cell autonomous effect on neuronal degeneration. A late conditional knock-out of TDP-43 in oligodendrocytes, the myelinating glial cells in the CNS, led to profound morphological changes, accompanied by abnormal myelination and splicing defects (Heo *et al*, 2022). The conditional knock-out of TDP-43 in SCs did not lead to

myelin defects or gross phenotypic changes; however, decrease in conduction velocity and altered clustering of paranodal proteins, with a splicing defect of neurofascin transcript were observed (Chang *et al*, 2021).

Aim

The aim of the present work was to evaluate if the pathological TDP-43 expression in SCs could contribute to neurodegeneration.

The project stemmed from the previous observation of TDP-43 pathology in SCs from motor nerves of living patients with ALS. We hypothesized that TDP-43 pathology might exert a non-cell autonomous effect on axons, contributing to neurodegeneration. To test this hypothesis, we decided to generate both an in vivo model and an in vitro model.

Mutations in the gene for the RNA-binding protein TDP-43 lead to amyotrophic lateral sclerosis (ALS), which is clinically and pathologically indistinguishable from most "sporadic" ALS cases, indicating that disrupted TDP-43 function and mislocalization are central drivers of neurodegeneration. Traditional transgenic mouse models that overexpress TDP-43 only partly mimic the key cellular features of human ALS and may introduce non-specific toxicity due to excessive protein levels.

Many previously described mouse models of TDP-43 proteinopathy are based on the overexpression of pathological TDP-43, sometimes with variants not reported in human disease, and this may introduce non-specific toxicity due to excessive protein levels. We chose to express human TDP-43 with the p.A382T mutation at near-normal level in SCs by integrating its sequence in the ROSA26 locus in a single copy. This mutation, which is associated with familial ALS and is the most prevalent TDP-43 mutation in Italian patients with ALS (Chiò *et al*, 2011), had never been previously expressed in a mouse model, either ubiquitously or in a selected cell-type. We decided to avoid the use of protein tags, since this might affect the aggregation properties of the protein; moreover, although the aminoacidic sequence of mouse, previous works reported the use of human-selective anti-TDP-43 antibodies in mouse models. As further explained in the methods section, we induced the selective expression of human TDP-43 p.A382T (or its wild-type counterpart, human TDP-43 WT) in SCs using a Cre-LoxP system.

In order to separately evaluate the cell autonomous effect of the expression of transgenic TDP-43, we also generated mice expressing the same transgenes in the motor neurons (MNs), using the same strategy.

For the in vitro model, primary fibroblasts were expanded from skin biopsies of living patients with ALS carrying the TDP-43 p.A382T mutation (and healthy controls) which had been previously performed. Induced pluripotent stem cells (iPSCs) were generated from these fibroblasts and then differentiated into spinal MNs or SCs. Using a previously described multicompartment microfluidic device, SCs with or without the TDP-43 mutation were co-cultured with MNs, in order to evaluate if the expression of TDP-43 p.A382T in SCs could have non-cell autonomous effect on MNs.

Methods

Project organization and work subdivision

Two units were involved in the project: the Experimental Neuropathology Unit (with two laboratories: one in IRCCS San Raffaele Institute, Milan, Italy; the other in Lecce, Italy); the Biology of Myelin Unit in IRCCS San Raffaele Institute, Milan, Italy.

The project included two branches: in vivo model and in vitro model.

The in vitro model was generated and studied at the Lecce branch of the San Raffaele Hospital laboratory. Although I did not take part directly to this side of the project, except for performing skin biopsies on ALS patients, we considered important to include it in the present thesis to provide a thorough perspective of the project.

During the first year of my PhD project, I attended the Lagier-Tourenne Lab at Massachusetts General Hospital, working with patient-derived ALS induced pluripotent cells (iPMN) and tissues from a mouse model of ALS. This experience provided me with the ability to work with cell models, perform protein and RNA extraction, immunostainings, as well as to learn different methods to study TDP-43 function in physiology and disease. Moreover, the obtained evidence supported the use of an in vitro model for the study of TDP-43 dysfunction at molecular level.

The in vivo model was generated and characterized at IRCCS San Raffaele Scientific Institute, from the collaboration between the Experimental Neuropathology Unit and the Biology of Myelin Unit.

Transgenic mouse model

The generation of the model was performed by Francesca Florio (Biology of Myelin Unit) with the support of the CFCM. Briefly, the protein coding sequence of the human TARDBP gene (hTDP-43) was obtained from a commercial plasmid (TDP43NOTAG1, #28206, Addgene) and inserted in a plasmid containing a loxP-flanked cassette with a PGK-neo selectable marker and a strong transcriptional stop sequence (pBigT, #21270, Addgene). The construct was then inserted in the

pROSA26-PA plasmid (#21271, Addgene). The pROSA26-PA plasmid contains the right and left arm of the ROSA26, allowing the insertion of the construct in this locus by homologous recombination. ROSA26 has a high endogenous expression level throughout development and is considered a "safe harbor" locus for transgene insertion (Soriano, 1999). The strong transcriptional stop sequence (triple SV40 polyadenylation sequence) prevents the expression of hTDP-43 until the co-expression of a Cre recombinase mediates the excision of the floxed sequence. hTDP-43 has no upstream promoter, the expression being guided by Rosa26 promoter after recombination.

To generate the p.A382T mutation (c.1144C>G), site-specific mutagenesis was performed on the final construct using the KODHotstartDNA polymerase (71086-3, Merck) with appropriate primers. The construct, with the p.A382T mutation or WT, was inserted in the Rosa26 locus by homologous recombination.

The construct was transfected by electroporation in the embryonic stem cells of a BalbC mouse. Neomycin and diphtheria toxin were used for positive and negative selection. Embryonic stem cells were then injected in a C57B/6 blastocyst and transferred to recipient pseudopregnant females. The resulting chimeras were crossed to C57B/6 mice to generate heterozygous hTDP-43 p.A382T (or WT) mice. Effective recombination of the transgene in the Rosa26 locus was verified by PCR.

Mpz-Cre (P0-Cre) mice were obtained from the Biology of Myelin lab of our institute (Feltri *et al*, 1999) whereas ChAT-Cre mice were purchased from Jackson laboratories (JAX:006410).

Heterozygous hTDP-43 p.A382T (or WT) mice were then crossed to P0-Cre mice, in order to generate heterozygous P0-Cre/ hTDP-43 p.A382T (or WT) mice.

hTDP-43 mice were not supposed to express the transgene and represented our control group to compare with P0-Cre/hTDP-43. P0-Cre/hTDP-43 WT mice were used to control whether the expression of the hTDP-43 transgene had an effect irrespective of the mutation.

To induce the selective expression of hTDP-43 in ChAT-positive neurons, hTDP-43 p.A382T (or WT) mice were crossed to ChAT-Cre mice. Genotype was confirmed by polymerase chain reaction (PCR) using the following primers: Rosa26 Fw GTCGCTCTGAGTTGTTATCAGTAAG; TARDBP Fw GGGATGAACTTTGGTGCGTTCAGC; Rosa26 Rev: CCTCCCATTTTCCTTATTTGCCCC; Mpz: CCACCACCTCTCCATTGCAC; Mpz-Cre: GCTGGCCCAAATGTTGCTGG

Dissections

Animals were sacrificed by carbon dioxide inhalation followed by neck dislocation at 6, 9, 12 and 18 months of age. A first group of animals was sacrificed at postnatal day 30 to assess hTDP-43 expression at RNA level.

For P0-Cre / hTDP-43 p.A382T (or WT) mice and littermates, we gathered sciatic nerves (mixed nerves), quadriceps branches of the femoral nerves (motor nerves), saphenous nerves (sensory nerves), extensor digitorum longus (a muscle with prevalence of fast glycolytic fibers) and soleus (a muscle with prevalence of slow oxidative fibers). For ChAT-Cre / hTDP-43 p.A382T (or WT) mice and littermates, we gathered also the spinal cord.

Sciatic nerves of each side were sampled between the hip and the thigh. The nerve sample (~1 cm) from each side was cut in halves and one half was snap frozen in liquid nitrogen for biochemistry analyses; the other half was fixed in 4% paraformaldehyde for 1 hour and then included in optimal cutting temperature (OCT) and frozen, or fixed in 2% glutaraldehyde for morphology studies and electron microscopy (see nerve morphology study). Quadriceps branches and saphenous nerves were dissected at thigh level with an optical microscope. Nerve samples were either snap frozen or fixed in 2% glutaraldehyde for morphology studies. Muscles samples (soleus and extensor digitorum longus) were fixed in fresh 4% paraformaldehyde for 1 hour, then washed in PBS and infiltrated with 20% sucrose for cryoprotection, then embedded in OCT and frozen. Spinal cord samples were cut in half; the half used for staining was fixed in a paraformaldehyde/glutaraldehyde mix, infiltrated in 20% sucrose and then embedded in OCT and frozen; the other half was snap frozen.

Nerve morphological study

For morphological studies, nerves fixed in glutaraldehyde 2% were post-fixed in osmium tetroxide 1%, dehydrated in ethanol gradient, included in Epon, and cut in 0.5 um semithin sections using a ultramicrotome. The semithin sections were stained with 2% toluidine blue in PBS for optical microscopy. The evaluated parameters included myelinated fiber density, axonal degenerations and G-ratio (inner diameter of the axon / total outer diameter of the axon and its myelin sheath), as well as a general overlook of the morphological appearance.

Morphological evaluation of the spinal cord included number and general appearance of neuronal somata in the anterior horns.

Nerve teasing

A sciatic nerve sample was put on a glass and a drop of PBS was poured on it. Under a stereoscopic microscope, the nerve fibers were dissected from the perineurium using fine tip needles. The glass was then left drying at RT for approximately 2 hours. The sample was then briefly fixed with cold acetone for 10 minutes. Immunostaining of teased nerves was performed with the same protocol used for regular nerve sections.

Immunostaining

For immunofluorescence of sciatic nerves, 4% PFA fixed nerves were included in OCT and then sectioned using a cryocutter, put on slides and frozen at -80°C until use. Samples were then thawed and dipped for 5 minutes in PBS to help remove the OCT. Nerve sections were circled using a hydrophobic pen. Blocking was peformed using 1% bovine serum albumin (BSA) added to a solution of 0.1% Triton-X in phosphate buffered saline (PBS) for 10 minutes. Sections were incubated overnight at 4°C with primary antibodies added to the blocking solution at the reported dilutions. On the second day of protocol, samples were rinsed in PBS and then incubated with secondary fluorescent antibodies at the reported dilution at room temperature (RT) for 1 hour. Samples were then rinsed in PBS and mounted with Vectashield DAPI before applying a cover glass. Images were taken using a Olympus BX51 fluorescence microscope.

Immunohistochemistry (for ChAT on spinal cord sections) was performed as follows: frozen OCT embedded sections were incubated with 3% hydrogen peroxide for 10 minutes, rinsed with ddH2O and blocked in 1% BSA + 0.1% Triton-X in PBS; then section were incubated with the primary antibody for 1 hour at RT, rinsed with PBS and incubated with the appropriate biotinylated secondary antibody for 1 hour at RT; then sections were incubated with Avidin-Biotin complex for 1 hour at RT, rinsed with ddH2O; finally, DAB was applied and sections were observed under an optical microscope until desired color intensity was reached.

Primary antibody list: Anti-TDP43 (Human specific) (Ms 1:100) Proteintech 60019-2-Ig;
Anti-TDP43 polyclonal (Rb 1:1,000) Proteintech 10782-2-AP; anti-phopsho(409/410)-TDP43 (Rb 1:1,000) Proteintech 22309-1-AP; Anti-Neurofilament M (Chk 1:800) BioLegend 822701; anti-CASPR (Rb 1:1,000) Abcam AB34151; anti-ChAT (Gt, 1:100)Millipore AB144P; anti-Zo-1 (Rb 1:1,000) Invitrogen 61-7300. Nuclei were stained with 4',6-diamidino-2-phenylindole (DAPI).

Secondary antibody list
anti-Mouse AlexaFluor 488 (Goat, 1:500) Invitrogen, A-11029; anti-Rabbit AlexaFluor 555 (Goat, 1:500) Invitrogen A-21428; anti-Chicken FITC (Donkey, 1:500), Jackson ImmunoResearch 703-095-155;

Transmission electron microscopy (TEM)

For electron microscopy, the Epon included nerve samples previously described in the nerve morphological study section were cut using a diamond-knife ultramicrotome (UC7, Leica Microsystem, Vienna, Austria) equipped with a 45° diamond knife (DiATOME, Nidau, Switzerland) in 80 nm sections and collected on a hexagonal 200-mesh grid for TEM. Sections were incubated for

5 minutes in a drop uranyl acetate and rinsed in distilled H2O; then incubated for 5 minutes with lead citrate and rinsed again in distilled H2O. Images were taken on a transmission electron microscope (CEM 902; Carl Zeiss).

Protein extraction and Western blot

Sciatic nerve or spinal cord samples were homogenized mechanically using ceramic beads (Precellys Lysing Kit, Precellys) with RIPA buffer (50 mM TrisHCl 1M pH 7.4; 150 mM; NaCl 5M; 10 mM EDTA 0.5M pH 8.0; 1% NP-40; 0.5% Na deoxycholate; 0.1% SDS) + protease inhibitor and phosphatase inhibitor. After centrifugation at 15,000 g at 4°C for 15 minutes, the soluble fraction was transferred to a new vial. Protein content was quantified using a commercial bicichoninic acid assay (Pierce BCA Protein Assay Kit, Thermofisher) as per vendor sheet. Protein samples were frozen at -80°C until use.

For western blotting, 50 ug protein with loading buffer (Laemmli buffer + 10% beta-mercaptoethanol) were denatured at 100°C for 5 minutes and loaded in the wells of a 12% SDS-PAGE gel. Proteins were then transferred on a PVDF membrane at 4°C for 1h at 100V. Ponceau S was applied on the membrane to visualize the protein bands. The membrane was then rinsed in PBS, blocked with 5% milk in PBS + 0.1% Tween-20 for 1 hour at RT and incubated on a rocker with the appropriate primary antibodies overnight at 4°C. On the following day, the membrane was rinsed and then incubated on a rocker with the secondary HRP-conjugated antibodies for 1 hour at RT. Images were taken on ChemiDoc BioRad system after adding ECL detection reagents to the membrane.

Primary antibody list
Anti-hTDP-43 (Ms 1:3,000) Proteintech 60019-2-Ig
Anti-GFAP (Rat 1:1,000) ThermoFisher 2.2B10
Anti-Neurofascin 155 (Chk 1:1,000) R&DSystems AF3235
Anti-Beta-III Tubulin (Ms, 1:1,000) Proteintech 66240-1-Ig

Secondary antibody list
anti-Mouse Ig HRP (Rat, 1:10,000) Agilent P0260002-2
anti-Rat Ig HRP (Goat, 1:5,000) Cell Signaling #7077
anti-Chicken Ig HRP (Goat, 1:2,500) Abcam ab6877

RT-qPCR (mouse samples)

Sciatic nerve or spinal cord samples were homogeneized mechanically using ceramic beads with Trizol in the Precellys Evolution device (Bertin technologies). RNA extraction was performed as per Trizol vendor protocol. RNA pellets were resuspended in 20 to 30 uL of RNase-free water and RNA concentration, 280/260, and 260/230 ratios were quantified on a spectrophotometer (MultiSky Scan, ThermoScientific).

500 ng RNA per sample were retrotranscribed to cDNA using the SuperScript™ II Reverse Transcriptase kit (Invitrogen), according to vendor protocol.

For the real-time quantification, reactions were manually assembled in a 96-well reaction plate and contained: 4uL of diluted cDNA (1:20 in distilled water), 12.5 uL master mix (Applied Biosystems™ TaqMan™ Universal PCR Master Mix), 1.25 uL TaqMan Gene Expression Assay (human TARDBP: Hs00606522_m1; mouse TARDBP Mm01256504_g1; 18S rRNA Hs99999901_s1; Applied Biosystems™). Every sample was analyzed in duplicate. 18S rRNA was used as internal control. Quantification was performed on a BioRad C1000Touch CFX96 system. Results were quantified using the ΔΔCt method.

Behavioral tests

Mice were evaluated at 6 months, 9 months, 12 months, and 18 months. Evaluations included Rotarod, inverted grid test, and clasping. Weight was measured on an appropriate scale before every testing session.

Rotarod: Mice underwent a training trial on a Rotarod (Ugo Basile) with a ramp speed from 2 to 20 rpm in 300 s. If an animal fell, the chronometer was stopped. The animals were considered trained after running for total 300 s. On the next three days, the latency to fall was recorded over three trials. Mice were first acclimated in the testing room for 10 minutes. The Rotarod was set at stable 4 rpm speed and the animals were placed on the spinning rod. Then, Rotarod was set for acceleration from 4 to 40 rpm over 300 s. Each trial was separated by at least 15 minutes rest. On the first day after training, the animals could fall 3 times per trial and be placed again on the rod before the trial was considered completed; on the second day, the animals could fall once; on the third day, the first fall stopped the trial. The average of the three measurements was used as the outcome value for each day.

Inverted grid test: mice were placed on the grid and accommodated at least 5 s. Then, the grid was inverted 40 cm above a box with bedding material for 180 s. Three trials, separated by at least 15 minutes, were repeated every day for two consecutive days. The holding impulse was calculated by multiplying the hanging time by the gravitational force of the mouse [body mass (g) x 0.00980665

N/g x hanging time (s)]. The average of the three measurements was used as the outcome value for each day.

Hindlimb clasping was testing by raising the mouse from near the base of the tail for 10 seconds and was rated according to the following scale: 0 (both hindlimbs splayed), 1 (one hindlimb is retracted toward the abdomen for more than 50% of the time suspended), 2 (both hindlimbs are partially retracted toward the abdomen for more than 50% of the time suspended), 3 (both hindlimbs are entirely retracted towards the abdomen for more than 50% of the suspension time).

Neurophysiology

The electrophysiological evaluation was performed with a specific EMG system (Neuro-MEP Micro, Neurosoft, Russia). Mice were anesthetized with ketamine 90ug/g + xylazine 10 ug/g of body weight and placed under a heating lamp to maintain constant body temperature. Sciatic nerve conduction velocity was obtained by stimulating the nerve with steel monopolar needle electrodes. A pair of stimulating electrodes was inserted subcutaneously near the nerve at the ankle. A second pair of electrodes was placed at the sciatic notch to obtain two distinct sites of stimulation, proximal and distal along the nerve. Compound motor action potential (CMAP) was recorded with a pair of needle electrodes; the active electrode was inserted in muscles in the middle of the paw, whereas the reference was placed in the skin between the first and second digits. Sciatic nerve F-wave latency measurement was obtained by stimulating the nerve at the ankle and recording the responses in the paw muscle, with the same electrodes employed for the nerve conduction velocity study.

Human iPSC generation and culture

Fibroblasts from patients with ALS carrying the TDP-43 p.A382T mutation and healthy donors (n= 2 and 2, respectively) were obtained by skin biopsy using a 2 mm punch under local anesthesia at IRCCS San Raffaele Scientific Institute. The dermis was dissected from the fat tissue, and fibroblasts were expanded in T25 flasks in DMEM culture medium. iPSCs were generated by our colleagues in Lecce using the CytoTune-iPS 2.0 Sendai Reprogramming Kit (ThermoFisher Scientific). Pluripotency of iPSC lines was tested using immunofluorescence assays and karyotyping. Human iPSC lines were cultured in feeder-free conditions using chemically defined mTeSR-1 medium on growth factor-reduced Geltrex-coated tissue culture plates. The medium was changed every other day, and colonies were split using the stem cell dissociation reagent EZ-LIFT (Sigma Aldrich). 60-80% confluent cultures were washed twice and then incubated at 37°C with EZ-LIFT™ reagent until a significant number of detached clumps were visible. Cells were gently collected with mTeSR-1 in a conical tube and centrifuged at 100g for 3 minutes. Pellets were resuspended in mTeSR-1™

supplemented with 5 μM ROCK inhibitor (RI) and plated on Geltrex-coated 6-well cell culture multiwell plates in a 1:5 split ratio. The medium was refreshed the following day. All the iPSC lines were periodically tested negative for Mycoplasma.

Differentiation of iPSC-derived motor neurons

iPSC-derived MNs (iMNs) were generated by our colleagues in Lecce using a previously published small molecule-based protocol (Du *et al*, 2015). Briefly, hiPSCs were plated on Geltrex-coated multi-well plates in mTeSR-1 medium with 5 μM RI. On the next day, medium was replaced with basal neural medium (BNM) [50% Neurobasal medium, 50% DMEM/F-12, 1% Pen/Strep, 1% Glutamine, 0.1 mM ascorbic acid, 0.5X N2, and 0.5X B27 supplement], adding 3 μM CHIR-99021, 2 μM dorsomorphin homolog 1 (DMH-1), and 2 μM SB431542. Fresh medium was added every other day until day 6, when cells were split with Dispase-II and plated in a 1:6 ratio. Then, BNM was supplemented with 1 μM CHIR-99021, 2 μM DHM-1, 2 μM SB431542, 0.1 μM retinoic acid (RA), and 0.5 μM smoothened agonist (SAG). Every other day, the medium was replaced until day 12. Subsequently, cells were split with Dispase-II and plated on ultra-low attachment multiwell in BNM supplemented with 0.5 μM RA and 0.1 μM SAG. On day 18, immature MN-spheres were dissociated with Accumax™, and single cells were plated on Geltrex-coated multiwell or glass in BNM supplemented with 0.5 μM RA, 0.1 μM SAG, and 0.1 μM Compound E. Finally, the medium was changed with fresh medium every other day until day 28.

Differentiation of iPSC-derived Schwann cells

iPSC-derived SCs (iSCs) were generated by our colleagues in Lecce using a previously published protocol (Kim *et al*, 2017). Briefly, iPSCs were cultured with a neural differentiation medium containing N2, B27, 20 uM SB431542, and 3uM CHIR99021 for 6 days; from day 6, Neuregulin-1 was added to the culture medium for the following 18 days to induce differentiation in SC precursors. SC precursors were then differentiated into immature SCs by adding NRG1 (200 ng/mL), RA (100 nM), PDGF (10 ng/mL) and forskolin (4 μM) to the differentiation medium for 3 days.

The microfluidic device was fabricated in collaboration with the CNR-Nanotec Institute in Lecce. The device is composed by three compartments (500 um width, 2.5um height, 6 mm length) with distinct inlets and outlets for fluid perfusion (diameter 2 mm) connected by microgrooves (5 um width, 2.5 um height, 50 um length) which allow the control of cellular migration and cell microenvironment (De Vitis *et al*, 2021).

For the co-culture experiment, SC precursors were seeded 2 days after the seeding of iMNs in an adjacent compartment and then differentiated into immature SCs during the following 8 days. The

third compartment of the device, in contact with the iMN compartment, contained only iMN differentiation medium.

Cell culturing in microfluidic devices

UV-sterilized microfluidic devices were equilibrated with distilled water at 37°C overnight and then coated with growth factor-reduced Geltrex. Before cell plating, devices were washed twice with DMEM/F-12. Then, the chambers of the chips were filled with culture media until the cells were seeded. Immediately before plating, culture media were removed from all reservoirs, ensuring that no bubbles were introduced. To plate MNs in chamber 2, cells were dissociated from neurospheres and concentrated to 5*10^6 cells/ml in MN medium supplemented with five 5 µM RI. A volume of 4 µl of concentrated MNs was pipetted into the entry port of the chamber. To plate SCPs in chamber 3, cells were concentrated to 1 × 10^6 cells/ml in SCDM1 and 6 µl of cell suspension were pipetted into the entry port of the chamber. After cell seeding, devices were transferred into the incubator for 1 hour, allowing cells to adhere. Thereafter, appropriate culture media were added to all reservoirs in equal volume.

Neurite length quantification

Neurites were analyzed with ImageJ software to quantify their length in chamber 3. An area of 8.26 cm width and 13.5 cm length of chamber 3 was selected as the region of interest (ROI). The NF-M signal of these areas was converted into binary images using the threshold ImageJ plugin, where black signals indicate the presence of axon processes. To quantify the total axon length in micrometers, the black signals were then skeletonized using the skeletonization ImageJ plugin.

Differentiation of iPSC-derived motor neurons (2)

During the first part of my PhD project, I differentiated iMNs using two different protocols.

A small molecule-based protocol was used to assess TDP-43 pathology after 6 weeks of differentiation (Coyne *et al*, 2020). Briefly, once iPSC colonies reached confluence in a 6-well plate (about 4-5 days after passaging), stage 1 medium consisting of 47.5% IMDM, 47.5% F12, 1% NEAA, 1% Pen/Strep, 2% B27, 1% N2, 0.2 µM LDN193189, 10 µM SB431542, and 3 µM CHIR99021 was added and exchanged daily until day 6. On day 6 of differentiation, cells were incubated in StemPro Accutase for 5 minutes at 37°C. Cells were collected from plates and centrifuged at 500 × g for 1.5 minutes. Cells were plated at 1 × 106 cells per well of a 6-well plate or 5 × 106 cells per T25 flask in stage 2 medium consisting of 47.5% IMDM, 47.5% F12, 1% NEAA, 1% Pen/Strep, 2% B27, 1% N2,

0.2 μM LDN193189, 10 μM SB431542, 3 μM CHIR99021, 0.1 μM all-trans RA, and 1 μM SAG. Medium was exchanged daily until day 12. On day 12 of differentiation, cells were switched to stage 3 medium consisting of 47.5% IMDM, 47.5% F12, 1% NEAA, 1% Pen/Strep, 2% B27, 1% N2, 0.1 μM Compound E, 2.5 μM DAPT, 0.1 μM db-cAMP, 0.5 μM all-trans RA, 0.1 μM SAG, 200 ng/mL Ascorbic Acid, 10 ng/mL BDNF, 10 ng/mL GDNF.

A shorter protocol based on the overexpression of transgenic transcription factors (Fernandopulle *et al*, 2018) was used to assess DPR synthesis and survival. Briefly, confluent iPSCs in a 6-well plate were collected and nucleofected with equal concentrations of PiggyBac hNIL donor and PiggyBac transposase plasmids (AddGene), using the Amaxa Nucleofector II Device (Lonza) and the Nucleofector Human Stem Cell Kit (Lonza). iPSC nucleofection was performed with the help of Dr. Xin Jiang and Dr. Su Min Lim. The hNIL construct is designed to allow the expression of the transcription factors NGN2, ISL1 and LHX3 in a Tet-ON system; it also includes a BFP reporter and a puromycin resistance to allow for selection. Two days after, medium was changed to iPSC medium + 5ug/mL puromycin to allow selection of nucleofected cells. Nucleofected iPSCs were then expanded to confluence and then replated (Day 0) in vitronectin-coated T75 flasks with induction medium (DMEM/F12 + 1% N2, 1% NEEA, 1% GlutaMax, 2 ug/mL doxycycline, and 0.1 ug/ mL compound E). After 3 days, cells were collected and replated in poly-L-ornithine coated plates (6 well-plates for protein and RNA collection, glass-bottom 96 well plates for imaging) with differentiation medium (Neurobasal medium + 1% N2, 1% NEEA, 1% GlutaMax, 0.2% BME, 1 ng/mL BDNF, 1 ng/mL GDNF, 1 ng/mL IGF-1, 1 ng/mL CNTF, 10 nM retinoic acid, 2 ug/mL doxycycline, and 0.1 ug/ mL compound E). Half medium changes were performed every 3 days. All cells were maintained at 37°C with 5% CO2. iPSCs and iPSC-derived motor neurons routinely tested negative for mycoplasma.

Dipeptide repeats mesurement

For DPR measurement, medium was removed, and cells were washed with PBS to remove cell debris. Radioimmunoprecipitation (RIPA) lysis buffer containing fresh protease and phosphatase inhibitors was added directly on the wells (~200 uL/well). The plates were kept on ice and swirled periodically for 15 minutes. Afterwards, lysed cells were aspirated and transferred to a 1.5 mL tube and centrifuged at 13,000 g for 12 minutes at 4°C. Supernatant was aspirated and protein concentration was measured by bicinchoninic acid assay. Poly(GP) and poly(GA) were measured in cell lysate using a sandwich immunoassay that utilizes Meso Scale Discovery (MSD) electrochemiluminescence detection technology as previously described (Gendron *et al*, 2017). The assay was kindly performed by dr.

Jensen-West at Mayo Clinic Jacksonville, Florida. The provided values are the mean of two reads performed from the same aliquot.

Survival assay

Survival assay was performed by counting nuclei. Since the PiggyBac hNIL donor plasmid includes a BFP, successfully nucleofected cells displayed blue-fluorescent nuclei, allowing us to count them. hNIL-nucleofected iPSCs were observed daily during the induction phase to make sure there had been no difference in nucleofection efficiency. hNIL motor neurons at Day 3 were seeded in a poly-L-ornithin coated glass-bottom 96-well plate at a density of 50,000 cells/well. Day 3 medium contained aphidicolin, a DNA polymerase inhibitor, in order to eliminate actively proliferating cells. At Day 6, cells underwent a full medium change, and a baseline count was performed. Counting was repeated on Day 8, Day 11, Day 14 and Day 17. For imaging, we used the ImageXpress Automated Cell Imaging System, taking 25 images with a 10x magnification in both brightfield and blue fluorescence (450 nm) spectrum, for each well of a 96-well plate. Four wells per genotype were longitudinally analyzed. For quantification, we used a custom MatLab script, gently provided by Aaron Held, by which we could perform image selection, stitching and counting.

RT-qPCR (iMN)

For RNA extraction, on the day of the experiment medium was removed, cells were washed in PBS and RNA was extracted using the ISOLATE II RNA Mini Kit (Bioline) according to the manufacturer instructions. RNA was quantified using a Nanodrop spectrophotometer.

First strand cDNA synthesis and oligo dT priming were performed using the High-Capacity cDNA Reverse Transcription Kit (Thermo) per manufacturer instructions. The quantitative PCR step was performed using the iTaqTM Universal Probes Supermix (Bio-Rad) and target specific TaqMan assays. GAPDH was used as endogenous control. Three technical replicates were assayed per biological sample and analyzed on a C1000 thermocycler with a 384-well qPCR reaction module (Bio-Rad). Results were quantified using the ΔΔCt method. All RT-PCR products were analyzed by electrophoresis on 2% agarose gels incubated with ethidium bromide for imaging.

Statistical analyses

Statistical analyses were performed in RStudio, version 2023.3.0.386.

T-test was used to compare means between two groups ANOVA followed by post-hoc Tukey HSD test was used to compare means between more than two groups (e.g. neurophysiological and

behavioral tests between genotypes). Kruskal-Wallis test with Dunn post-hoc test was used when the sample size was too low to perform parametric tests.

Results

In vitro model

Differentiation of human iPSCs into motor neurons

We differentiated iPSCs from a patient with ALS carrying a C9ORF72 hexanucleotide repeat expansion, a mutation which is associated to TDP-43 pathology, into induced spinal motor neurons (C9-iMNs). iMNs obtained from iPSCs of an age-matched healthy subject were used as a control. A small molecule-based protocol and a transcription factor (human NGN2, ISL1 and LHX3, denominated hNIL factors) overexpression-based protocol were used in parallel, as further explained in the method section. The small molecule differentiation protocol is based on a series of sequential and overlapping steps that employ a combination of small molecules capable of modulating specific key signaling pathways and incorporates distinct processes that recapitulate motor neuron development. The initial step of the differentiation process focused on the induction of neural fate and caudalization, through dual SMAD inhibition. This is followed by proliferation and ventralization, induced by activation of the SHH pathway. Then, motor neuron precursor differentiation into motor neurons is induced. In the hNIL differentiation protocol instead, a construct containing three key transcription factors for motor neuron differentiation is nucleofected in iPSCs. The construct is designed to allow the expression of the transcription factors in a Tet-ON system, and contains a blue-fluorescent protein (BFP) reporter to help in the selection process. Then, nucleofected iPSCs are differentiated in a culture medium containing doxycycline and small molecules.

Successful differentiation of iMNs was confirmed by staining for neuronal and motor neuronal markers, including Tubulin BIII and Isl-1 (Figure 1A). In C9ORF72-ALS, the common neuropathological hallmark of TDP-43 pathology is accompanied by the synthesis of toxic dipeptide repeats, which are translated from the hexanucleotide repeat expansion. Among these, the most abundant are poly-glycine-proline (poly-GP) and poly-glycine-alanine (poly-GA). By using an immunochemical assay, we could detect dipeptide repeats poly-GP and poly-GA in the lysate of C9-iMNs, which were substantially absent in control iMNs (Figure 1B); poly-GP and poly-GA were detectable in C9-iMN lysate irrespective of the differentiation protocol. We evaluated iMN survival, taking advantage of the BFP reporter inserted in the hNIL construct. After plating cells at an equal

density, C9-iMNs showed reduced survival compared to control iMNs (Figure 1C). C9-iMNs did not show overt TDP-43 mislocalization at immunocytochemistry and we could not observe aggregation of TDP-43, even though signal quantification suggested an altered nuclear to cytoplasmic TDP-43 ratio in C9-iMNs obtained with the hNIL overexpression differentiation protocol (Figure 1D). We then tried to investigate if any sign of TDP-43 dysfunction was detectable in C9-iMNs. STMN2 is one of the most expressed genes in human motor neurons. The splicing of STMN2 is modulated by TDP-43 in human motor neurons, and loss of TDP-43 function induces the inclusion of the cryptic exon 2a in STMN2. The inclusion of the cryptic exon generates a premature transcriptional stop signal, leading to the synthesis of a truncated transcript and to reduced levels of functional protein. RT-qPCR performed in iMNs obtained with the small molecule differentiation protocol showed the presence of STMN2 cryptic exon after 6 weeks of differentiation, even though we did not observe significant reduction in STMN2 full length transcript (Figure 1E).

In conclusion, we observed disease-related molecular alterations in C9-iMNs, associated to a survival defect. Moreover, our results suggest that TDP-43 dysfunction is detectable in ALS patient-derived iMN, even in absence of overt TDP-43 pathology.

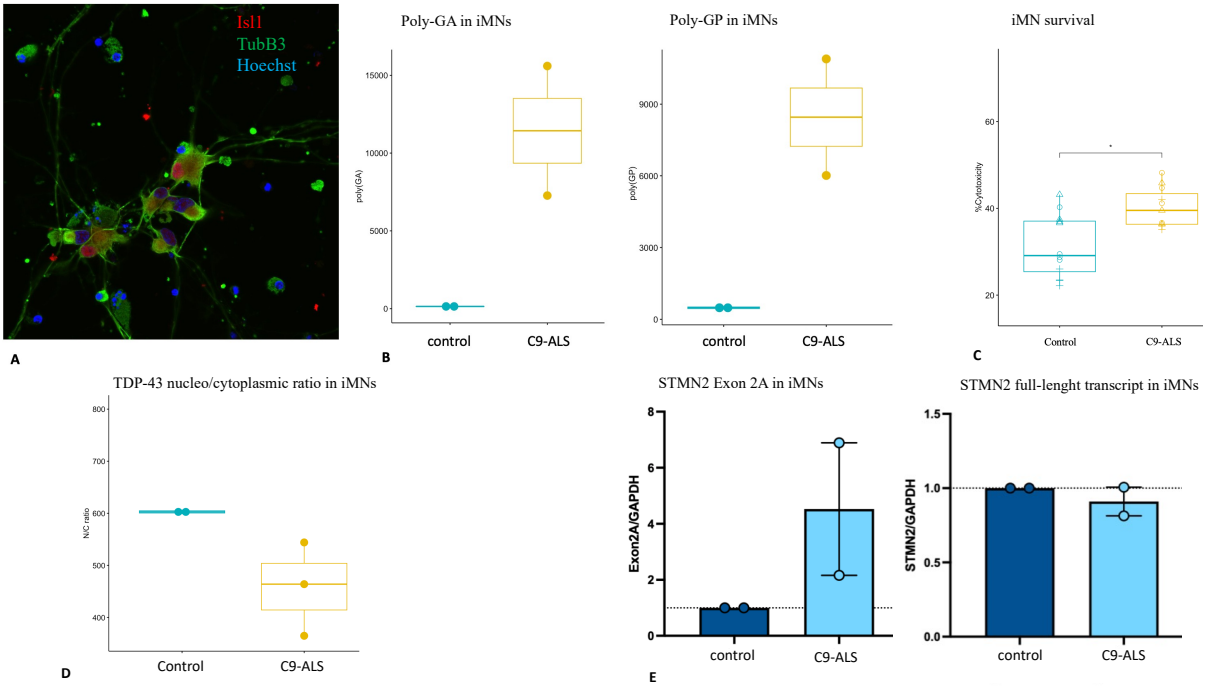

Figure 1: ***C9-iMNs show specific pathology, survival defect, and TDP-43 dysfunction*** *Immunocytochemistry for Isl1 (red), and beta3-tubulin (green) shows efficient differentiation of iMN (**A**); the image represents iMNs obtained with the small molecule differentiation protocol after 4 weeks of differentiation. Quantification by MSD-Mesoscale of dipeptide repeats poly-GA and poly-GP in iMN lysate; each dot is a biological replicate (**B**). Evaluation of iMN survival by nuclei counting (% relative to initial count after 10 days of differentiation) (**C**). Quantification of TDP-43 signal by immunocytochemistry shows reduced nuclear/cytoplasmic TDP-43*

*ratio in C9-iMNs, suggesting TDP-43 mislocalization (**D**). RT-qPCR for STMN2 Exon 2A and STMN2 full-length transcript in iMNs obtained with the small molecule differentiation protocol after 6 weeks of differentiation; expression level was normalized to GAPDH (**E**).*

In parallel, our colleagues in Lecce differentiated iMN from iPSCs obtained from a patient with ALS carrying the TDP-43 p.A382T mutation and a healthy donor. A small molecule-based differentiation protocol, similar to the one used for C9-iMNs, was followed as explained in the method section. iMNs expressed cell-type specific markers confirming successful differentiation (Figure 2A). The presence of the TDP-43 p.A382T mutation did not affect differentiation efficiency. iMNs did not manifest features of TDP-43 pathology, such as nuclear depletion or cytoplasmic aggregation of TDP-43, in physiological conditions. Interestingly, STMN2 cryptic exon 2a was detectable in TDP-43 p.A382T iMNs, even though STMN2 full-length transcript levels were unchanged, similarly to what we observed in C9-iMNs (Figure 2B).

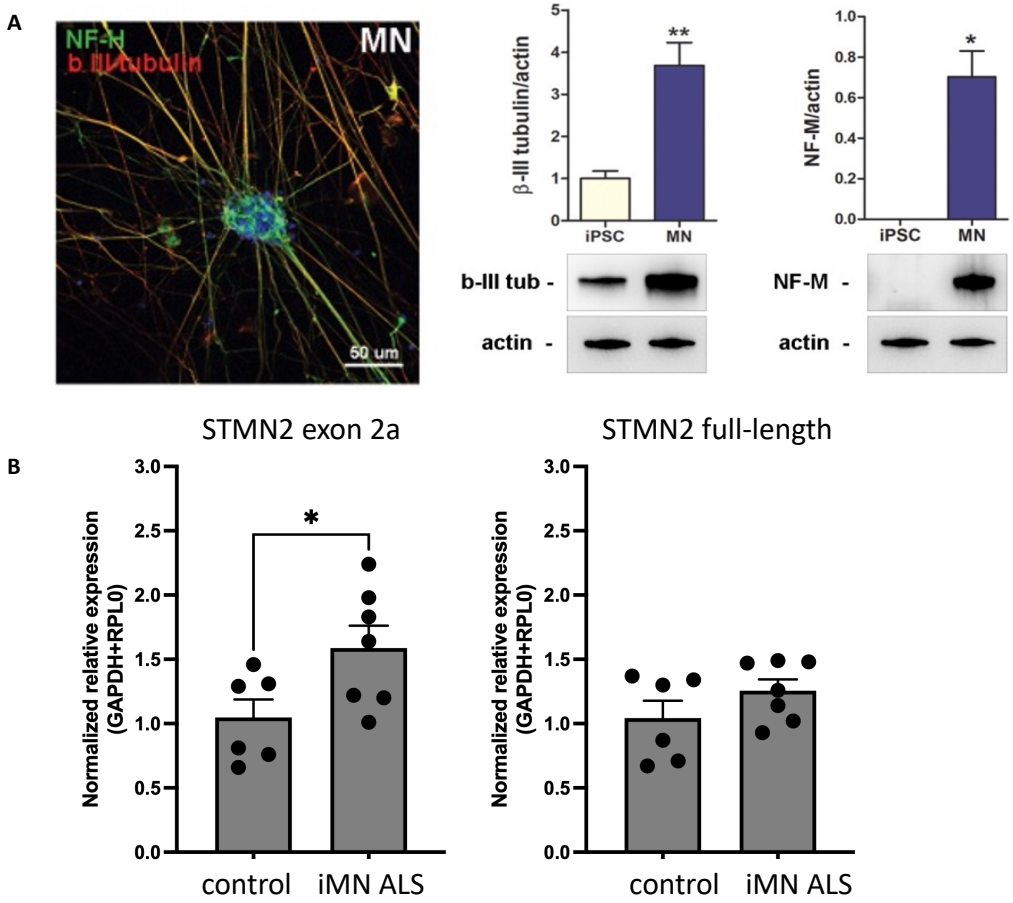

Figure 2: ***TDP-43 p.A382T iMNs show TDP-43 dysfunction.*** *In the upper part of the figure, differentiation of motor neurons is confirmed by cell-type specific markers in immunocytochemistry and Western blot (**A**). In the lower part of the figure, RT-qPCR detected higher levels of STMN2 exon 2a in TDP-43 p.A382T iMNs*

*compared to control iMNs, although STMN2 full-length transcript levels were comparable; each dot corresponds to a biological replicate (**B**).*

Differentiation of human iPSCs into Schwann cells

The differentiation of human iPSC into Schwann cells was performed entirely at our fellow laboratory in Lecce. Starting from skin fibroblasts of a healthy donor, iPSCs were obtained using a Sendai Reprogramming Kit. Then, a previously published protocol (Kim *et al*, 2017) was followed in order to differentiate induced SCs, as shown in Figure 3A.

The differentiation of iPSCs in SC precursors was evaluated by cell morphology and expression of specific markers SOX10 and NGFR by immunocytochemistry. Afterwards, SC precursors were differentiated in immature SCs using a differentiation medium containing NRG1 (200 ng/mL), RA (100 nM), PDGF (10 ng/mL) and forskolin (4 µM). After a week, SC precursors developed a spindle-like morphology and expressed specific markers GFAP and OCT6 in immunocytochemistry (Figure. 3B). Differentiation was confirmed by expression of CDH19 and ErbB3 at Western blot (Figure 3C).

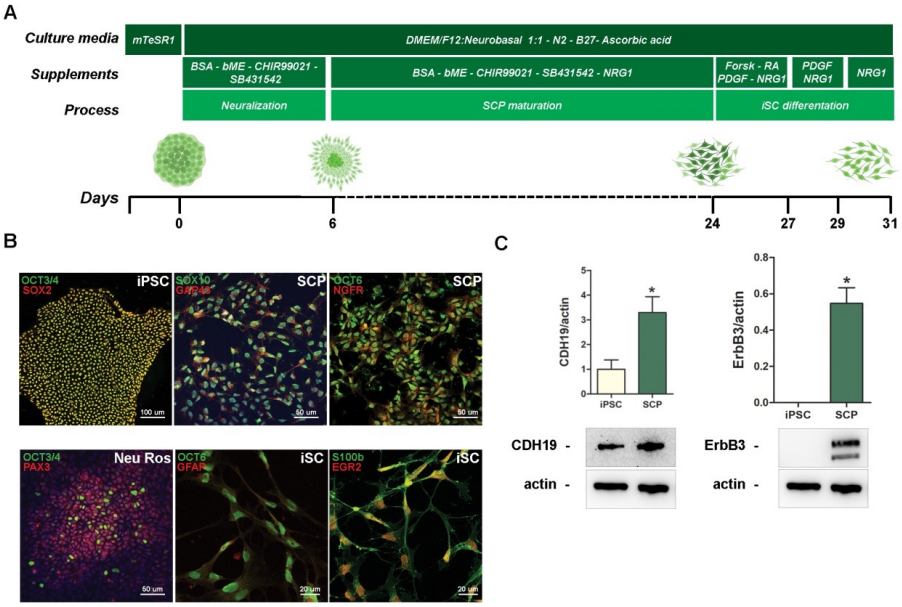

Figure 3: ***Generation and characterization of iPSC-derived Schwann cells*** *Graphic summary of the differentiation protocol (**A**). Expression of specific markers of differentiation at iPSC, SPC (Schwann cell precursor) and immature Schwann cells (iSC) state, evaluated by immunocytochemistry (**B**) and Western blot (**C**).*

Co-culture of iPSC-derived SCs and MNs

The co-culture of SCs and MNs was performed entirely at our fellow laboratory in Lecce.

In order to test whether TDP-43 dysfunction in the SC has a non-cell autonomous effect on MNs, our collaborators in Lecce co-cultured induced SCs (iSCs) with iMNs.

To model the spatial organization of the motor unit, we used a microfluidic culture device subdivided in three compartments (Fig. 4A). iPSC were differentiated into iMN in the central compartment. Induced SC precursors were seeded after three days in the adjacent communicating compartment. A third communicating compartment, adjacent to the iMN compartment, contained only iMN differentiation medium. Importantly, these chambers are interconnected with parallel microgrooves that serve to compartmentalize MN somas while allowing axons and dendrites to extend into neighboring compartments. Immunostaining confirmed the differentiation of SC precursors into pre-myelinating immature SCs after 10 days of differentiation. iSCs migrated along and reached contact with the growing axons, although myelination was not observed. iMN axons grew towards the iSC compartment and not towards the compartment containing medium without cells. Thus, neurite outgrowth is specifically dependent on the presence of SCs, underscoring their pivotal role in this process.

Since our goal was to test the non-cell autonomous effect of the expression of TDP-43 p.A382T in SCs, we also differentiated SCs from cells of patients with ALS harboring a TDP-43 p.A382T variant. The presence of the variant did not impact the differentiation process.

We proceeded to investigate the interaction between axons and SCs, utilizing the microfluidic device in conjunction with iMNs and SCs obtained from an ALS patient carrying the p.A382T mutation in the TARDBP gene. Four coculture conditions were established within our device: fully controlled setups using healthy MNs and healthy SCs; fully mutant configurations involving ALS MNs and SCs; and hybrid combinations including healthy MNs paired with ALS SC or vice versa. An immunofluorescence assay was performed to evaluate interactions between iMNs and iSCs using neurofilament as a marker for MNs and SOX10 as a marker for SCs. Neurite outgrowth was quantified by measuring the area occupied by neurites in the co-culture compartment.

Compared to iMN co-cultured with control induced SCs, iMN co-cultured with TDP-43 p.A382T SCs had a significant reduction in axonal growth. The presence of the TDP-43 p.A382T mutation also had a cell autonomous toxic effect on iMNs, which displayed reduced when co-cultured with iSC both with or without the mutation (Fig. 4B).

This result suggests that TDP-43 dysfunction in SCs might affect axonal growth and survival.

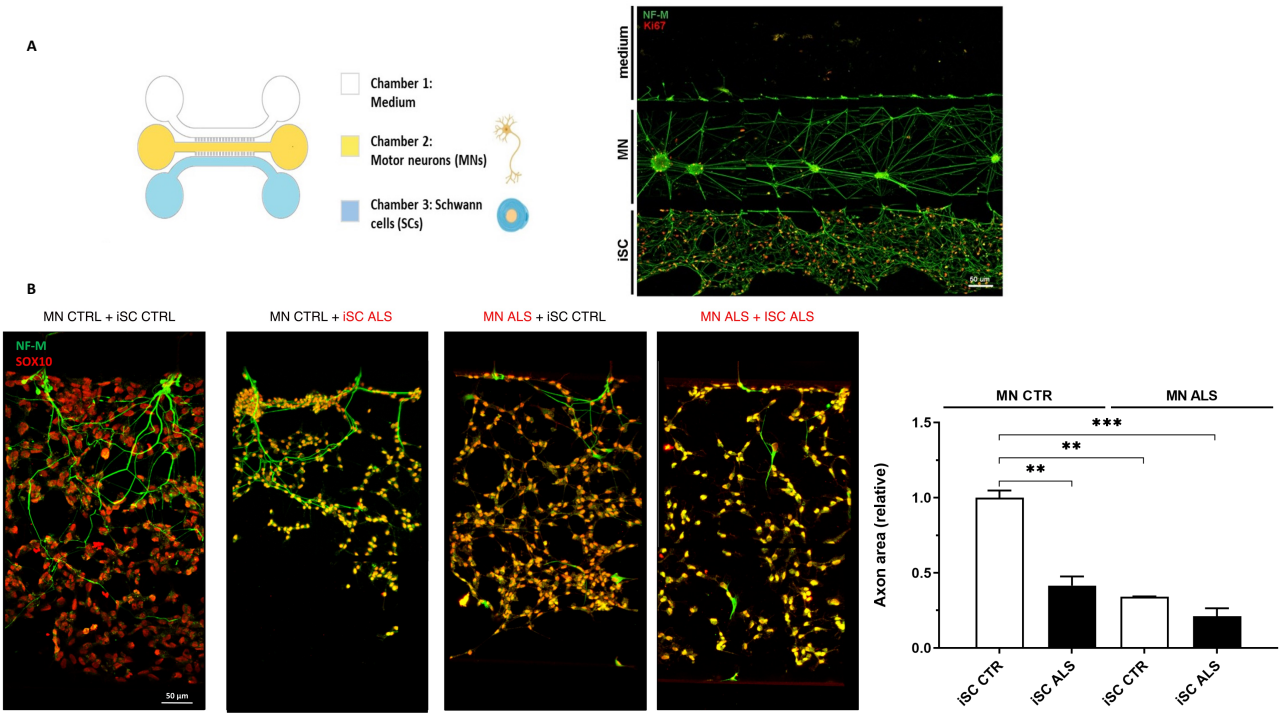

Figure 4: ***Schwann cells with the TDP-43 p.A382T impair axonal growth in vitro.*** *In the upper part of the figure, a scheme of the spatial organization of our microfluidic device (**A**). In the lower part of the figure, immunostaining for axonal marker NF-M (green) and SC cell marker SOX10 (orange) shows significantly decreased axonal growth in chamber 3 when control iMNs are co-cultured with iSC carrying the TDP-43 p.A382T mutation. The presence of the mutation decreases axonal growth also when expressed in iMNs only, as shown in the quantification on the right ($p<0.01$).*

In vivo model

Generation of the in vivo model

To explore the pathogenic properties of TDP-43 p.A382T, we generated transgenic mice selectively expressing the mutated human TARDBP gene (hTDP-43 p.A382T), or its wild-type counterpart (hTDP-43 WT), in the SC, as explained more thoroughly in the method section. The human transgene was preceded by a floxed transcriptional stop signal; in this way, only the presence of a Cre recombinase could induce the expression of the transgene. The construct was inserted in the ROSA26 locus to prevent off target recombination events and induce near-normal expression level. Mice harboring the transgene with the floxed stop signal (hTDP-43 mice) were crossed to mice expressing the Cre recombinase under the control of the myelin protein zero promoter (P0-Cre mice). The resulting offspring included the P0-Cre/hTDP43 p.A382T mice, which were designed to constitutively express the human transgene only in SCs, since the expression of the Cre recombinase was under the control of the P0 promoter, at a near-physiological level. hTDP-43 p.A382T mice were

used as controls, along with wild-type mice. The generation of the model is presented graphically in Figure 5.

P0-Cre/hTDP-43 WT mice were also generated, together with the respective hTDP-43 WT controls, in order to evaluate the effect of the expression of the human WT transgene in the same cells.

ChAT-Cre/hTDP-43 p.A382T and ChAT-Cre/hTDP-43 WT mice were generated to study the effect of the transgene expression in cholinergic neurons. The aim was to model the cell autonomous effect of the expression of the human transgene, since spinal motor neurons express choline acetyltransferase (ChAT).

Transgenic mice were vital, were born in the expected mendelian ratio, had a similar weight at birth compared to control and WT mice and were overall phenotypically normal, without showing gross malformations or behavioral abnormalities. The sample size for subsequent behavioral and neurophysiological characterization counted at least 30 mice per time point (approximately 10 per genotype) equally divided by sex.

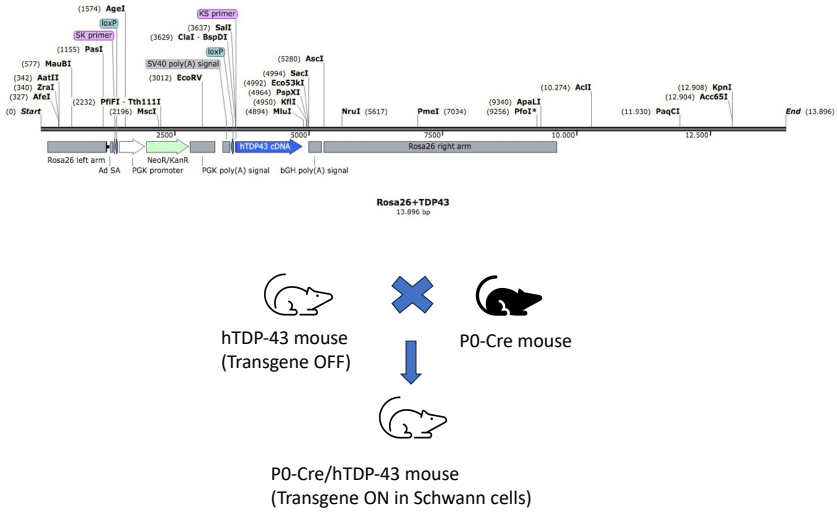

Figure 5: ***Graphic summary of the mouse model.*** *The upper part of the figure shows the construct, designed for integration in Rosa26. The transgene (hTDP43 cDNA) is preceded by a floxed (as shown by loxP sites on each side) neomycin resistance cassette with a transcriptional stop signal, which prevents the transgene expression. In the lower part of the figure, P0-Cre/hTDP-43 mice express the Cre recombinase in Schwann cells, where the floxed sequence is then excised, activating the transgene expression in a cell-type specific manner.*

Behavioral characterization of P0-Cre/hTDP-43 mice

We characterized P0-Cre/hTDP-43 A382T mice by three different behavioral assessments, namely hindlimb clasping, hanging grid test, and Rotarod, at four different timepoints (6, 9, 12 and 18

months). Three Rotarod trials were performed over three consecutive days after one day of training, and time to fall was recorded as explained in the method section. For the hanging grid test, time to fall was recorded for three trials over two consecutive days; time to fall was normalized to mouse weight at the time of testing. Hindlimb clasping was testing by raising the mouse from near the base of the tail and was rated on a 0 (absent) to 3 (both hindlimbs are entirely retracted for most of the suspension time).

P0-Cre/ hTDP-43 A382T mice did not show any significant difference at any timepoint in their performance compared with control hTDP-43 A382T mice and WT mice (Figure 6). Comparably, P0-Cre/hTDP-43 WT mice did not show any significant difference in their performance compared with control hTDP-43 WT and WT littermates.

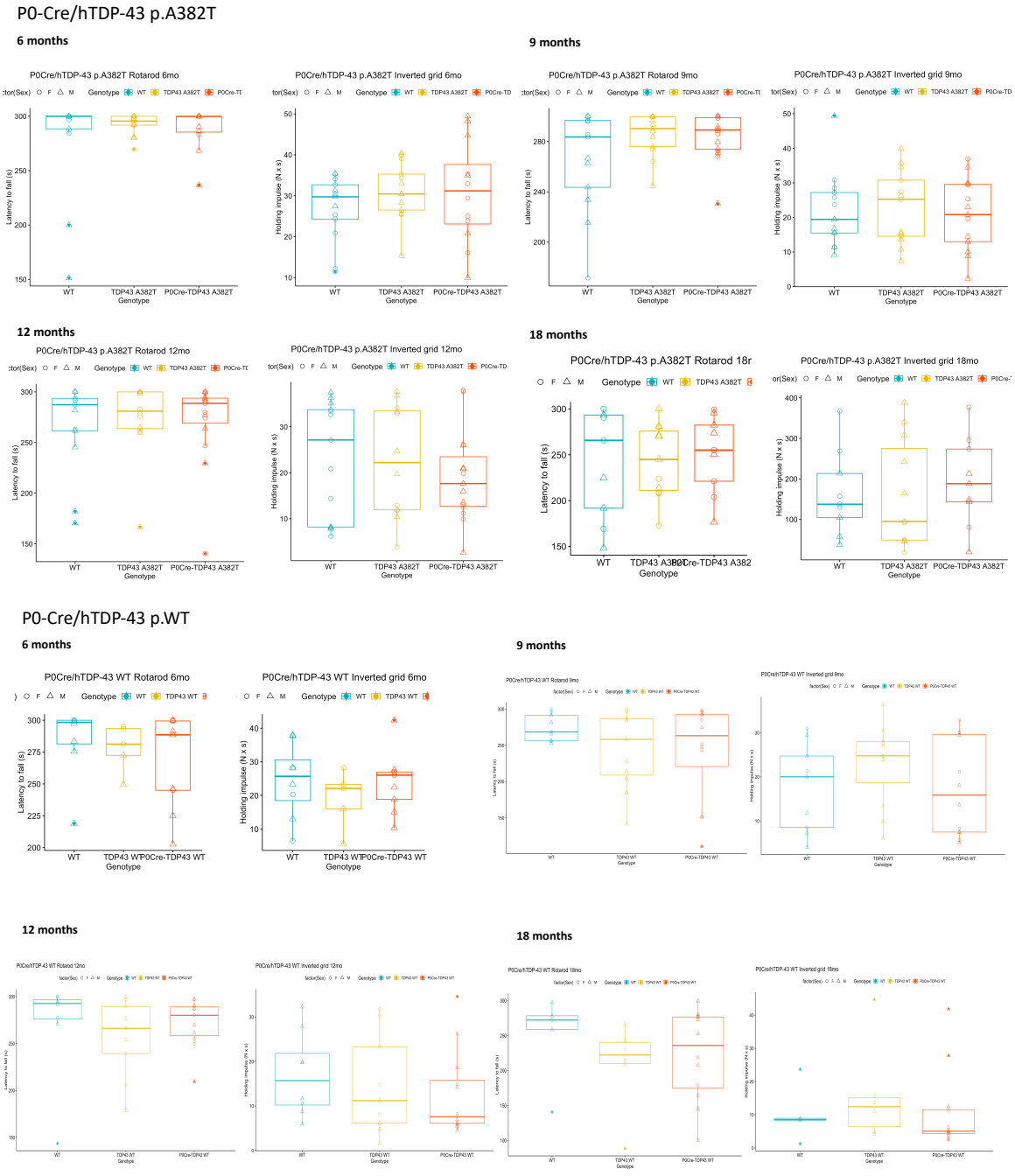

Figure 6: ***Results of the behavioral tests.*** *We evaluated Rotarod and inverted grid test. Each dot corresponds to the mean performance of a mouse per timepoint. The figure shows the results of neurophysiological tests in P0-Cre/hTDP-43 p.A382T mice (upper part of the figure) and in P0-Cre/hTDP-43 WT mice (lower part of the figure) at 6 months, 9 months, 12 months, and 18 months.*

Neurophysiological characterization of P0-Cre/hTDP-43 mice

We assessed nerve conduction by nerve conduction study at four different timepoints (6, 9, 12 and 18 months). We specifically tested parameters evaluating both axonal and myelin integrity. F-waves are a late motor response induced by supramaximal electrical stimulation of a motor nerve, which results in an antidromic stimulus and generates a reflex-like response in motor neuron pools; an increased latency of the F-wave can be the result of an alteration in nerve conduction along the nerve. The amplitude of the coumpound motor action potential (cMAP) depends on the number of motor axons in the nerve and can be decreased if motor axons degenerate. Motor nerve conduction velocity is measured between two discrete points of a motor nerve and can be decreased in consequence of altered myelination. P0-Cre/ hTDP-43 A382T mice did not show any significant difference in the evaluated nerve conduction parameters (F-wave latency, cMAP amplitude, and conduction velocity) compared with control hTDP-43 A382T mice and WT mice; a non-significant trend (ANOVA p= 0.06) for lower cMAP amplitude in P0-Cre/hTDP-43 p.A382T was observed by 18 months of age. Comparably, P0-Cre/hTDP-43 WT mice did not show decreased motor action potential amplitude, increased F-wave latencies or a slower conduction velocity in their nerve conduction studies compared with control hTDP-43 WT and WT littermates. Results are shown in Figure 7.

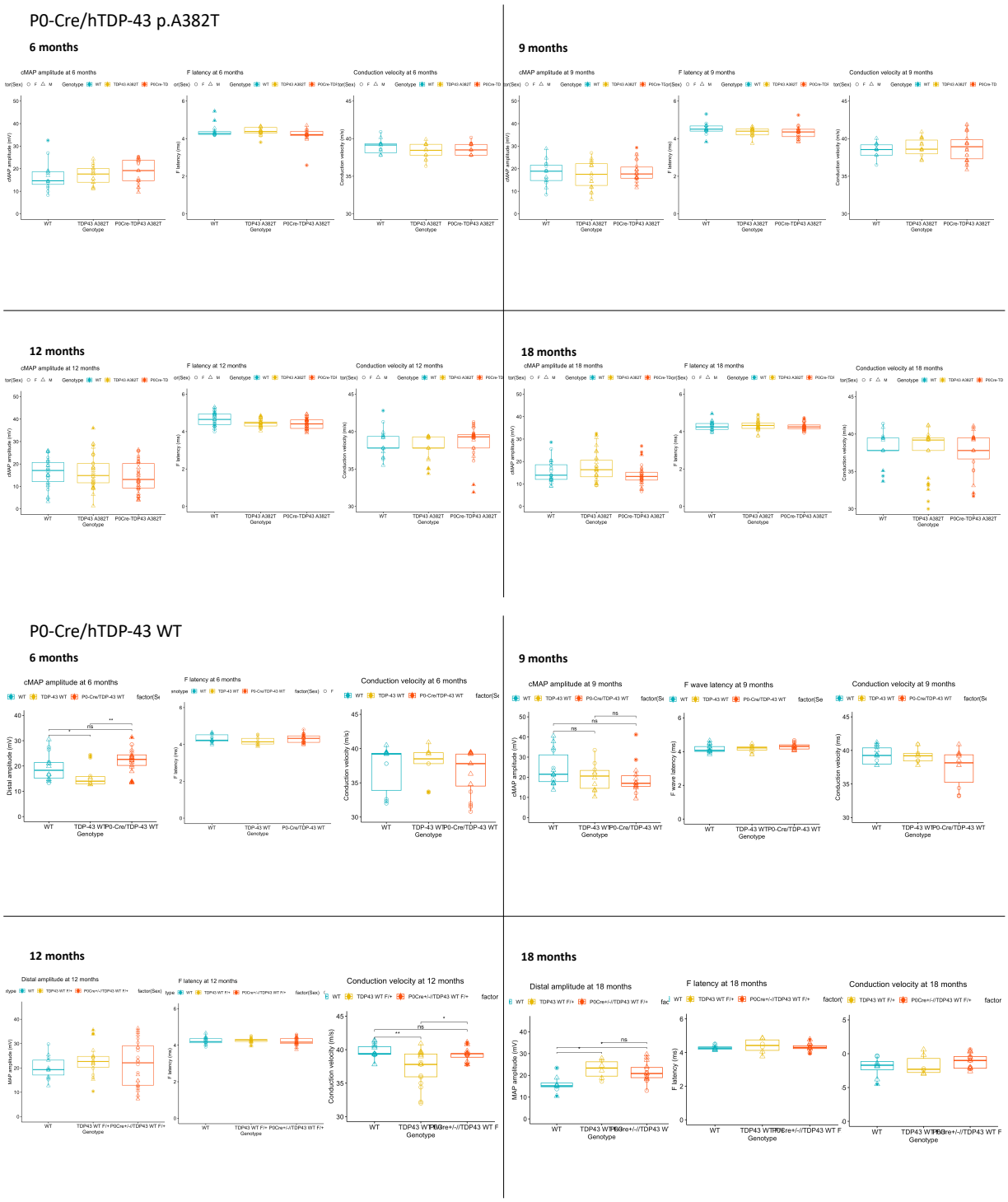

Figure 7: ***Results of the neurophysiological tests.*** *We evaluated distal cMAP amplitude, F wave latency and conduction velocity from the sciatic nerves. Each dot corresponds to the registration from a hindlimb. The figure shows the results of neurophysiological tests in P0-Cre/hTDP-43 p.A382T mice (upper part of the figure) and in P0-Cre/hTDP-43 WT mice (lower part of the figure) at 6 months, 9 months, 12 months, and 18 months.*

Neuropathological characterization of P0-Cre/hTDP-43 mice

Peripheral mixed (sciatic), motor (quadriceps branch of the femoral nerve) and sensory (saphenous) nerves were evaluated morphologically by toluidine blue staining of semithin sections at four different timepoints (6, 9, 12 and 18 months).

No morphological abnormality was observed at 6 months of age in P0-Cre/hTDP-43 p.A382T mice, hTDP-43 p.A382T littermate controls or WT mice, as well as in P0-Cre/hTDP-43 WT mice and relative controls, in mixed, motor or sensory nerves.

At 9 months of age, P0-Cre/hTDP-43 p.A382T mice did not show significant differences in myelinated fiber density compared to control or WT mice, a finding compatible with the normality of neurophysiological tests; however, sparse nerve fibers with an abnormally thin myelin were noted in sciatic and quadriceps nerves (Figure 8A). No alteration was observed in sensory nerves. These findings were confirmed at electron microscopy imaging (Figure 8B).

Despite not showing a significant difference in myelinated fiber density compared to control or WT mice, P0-Cre/hTDP-43 p.A382T mice sporadically displayed bizarre formations, such as double myelinations and morphologically altered paranodes, along with sparse axonal degenerations and onion bulbs, at 12 months of age in sciatic and quadriceps nerves (Figure 9A). Electron microscopy confirmed abnormal findings, including bizarre double myelinations (Figure 9B), and showed altered spatial organization of SC microvilli at the node of Ranvier level (Figure 9C). These alterations affected only few fibers and were not found in all samples. P0-Cre/hTDP-43 WT mice and relative littermate controls did not display any relevant abnormality.

At 18 months of age, P0-Cre/ hTDP-43 p.A382T mice still showed sporadic axonal degenerations (Figure 10A). Interestingly, abnormal regenerating clusters of nerve fibers were observed at epineural level in sciatic nerves of P0-Cre/ hTDP-43 p.A382T mice at this timepoint (Figure 10B), suggesting previous axonal damage and possibly impaired perineurial function; alterations of the perineurium were also observed at electron microscopy (Figure 10C).

P0-Cre/hTDP-43 WT mice did not display relevant morphological finding compared to littermate controls at 18 months and at previous timepoints.

In conclusion, P0-Cre/hTDP-43 p.A382T mice developed adult-onset sparse pathological nerve alterations, affecting axon-myelin interplay and fascicle organization. P0-Cre/hTDP-43 WT mice did not display any significant qualitative or quantitative morphological alteration.

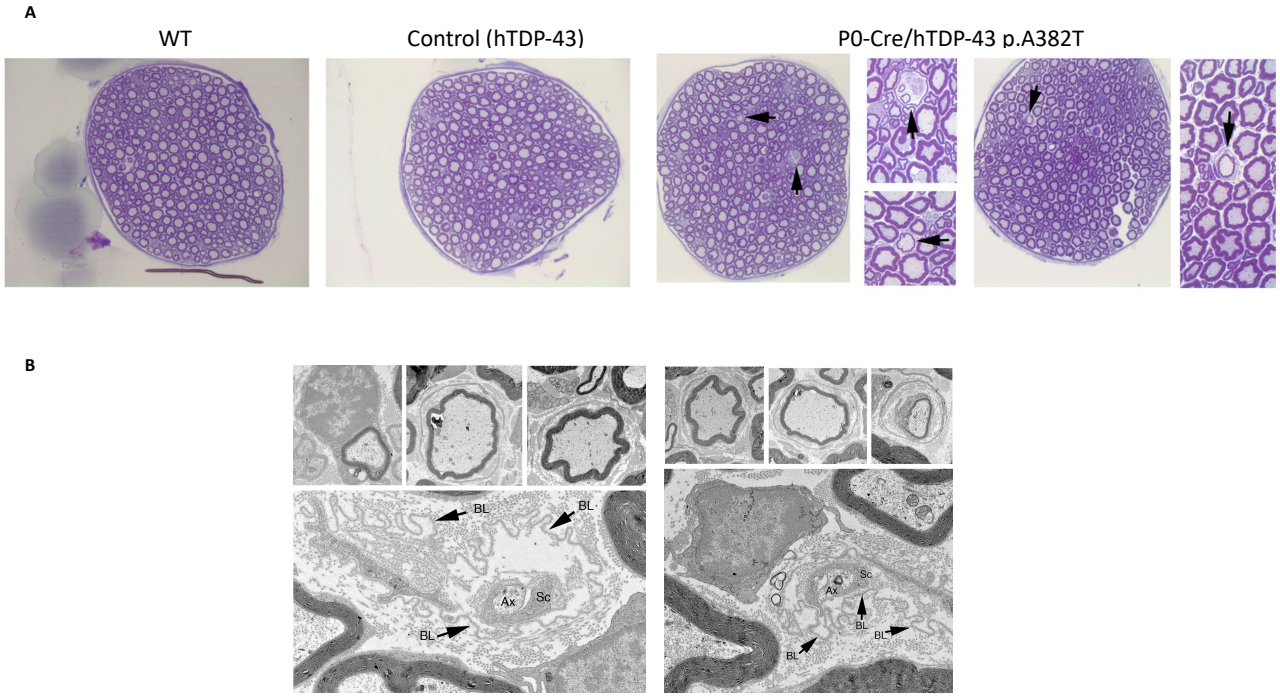

Figure 8: ***Morphological and ultrastructural analyses at 9 months.*** *In **A**, quadriceps nerve sections of P0-Cre/hTDP-43 p.A382T mice show sporadic hypomyelinated fibers and onion bulbs, suggesting myelination impairment, which were absent from control mice. Arrows indicate a fiber with thin myelin and an onion bulb. In **B**, electron microscopy shows a demyelinated SC-axon unit. BL: Schwann cell basal lamina; Ax: axon.*

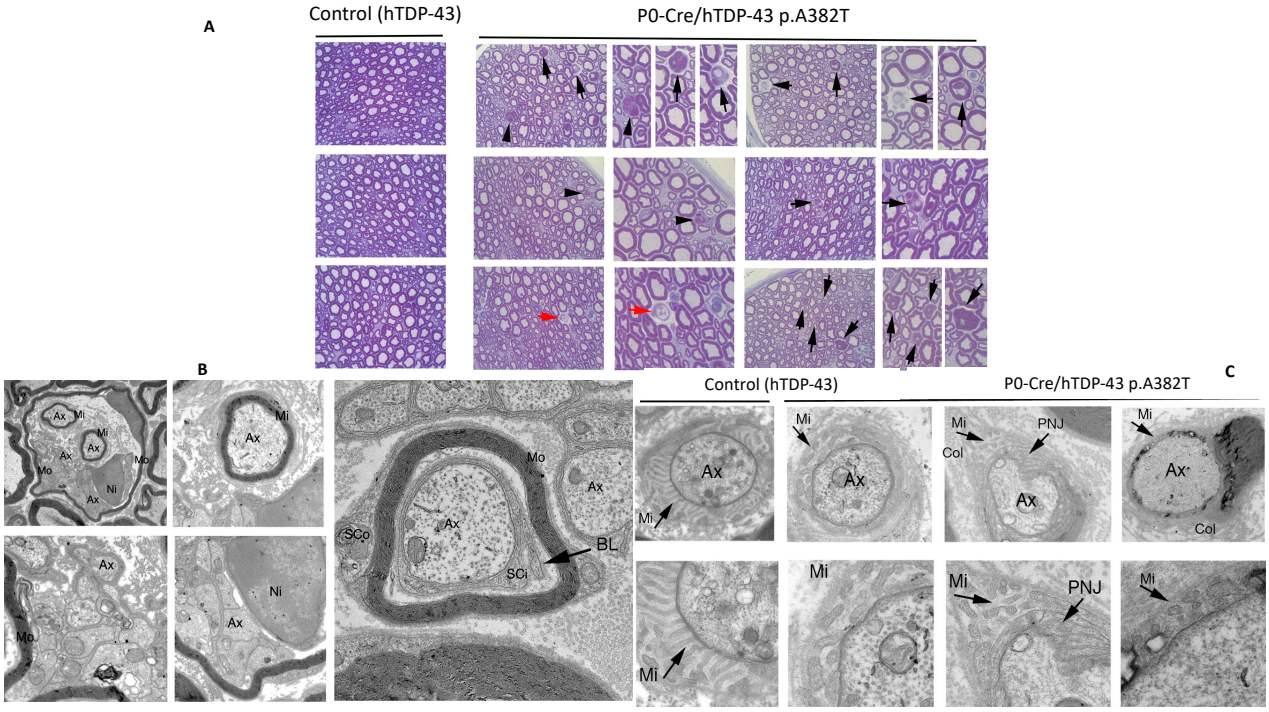

Figure 9: ***Morphological and ultrastructural analyses at 12 months.*** *In **A**, sciatic nerve sections of P0-Cre/hTDP-43 p.A382T mice show sporadic morphological abnormalities of the paranodes (arrows), axonal degenerations (arrowpoints), and hypomyelinated fibers (red arrows), which were absent from control mice. In **B**, electron microscopy shows on the left side a bizarre formation composed by an outer myelin sheath (Mo),*

enclosing three axons (Ax), of which two are myelinated (Mi); on the right an axon enveloped by an "inner" non-myelinating Schwann cell (SCi) with its own basal lamina (BL) and an outer myelinating Schwann cell (SCo). Abnormal spatial organization of SC microvilli (Mi) at node of Ranvier level is shown in ***C****. PNJ: paranodal junction.*

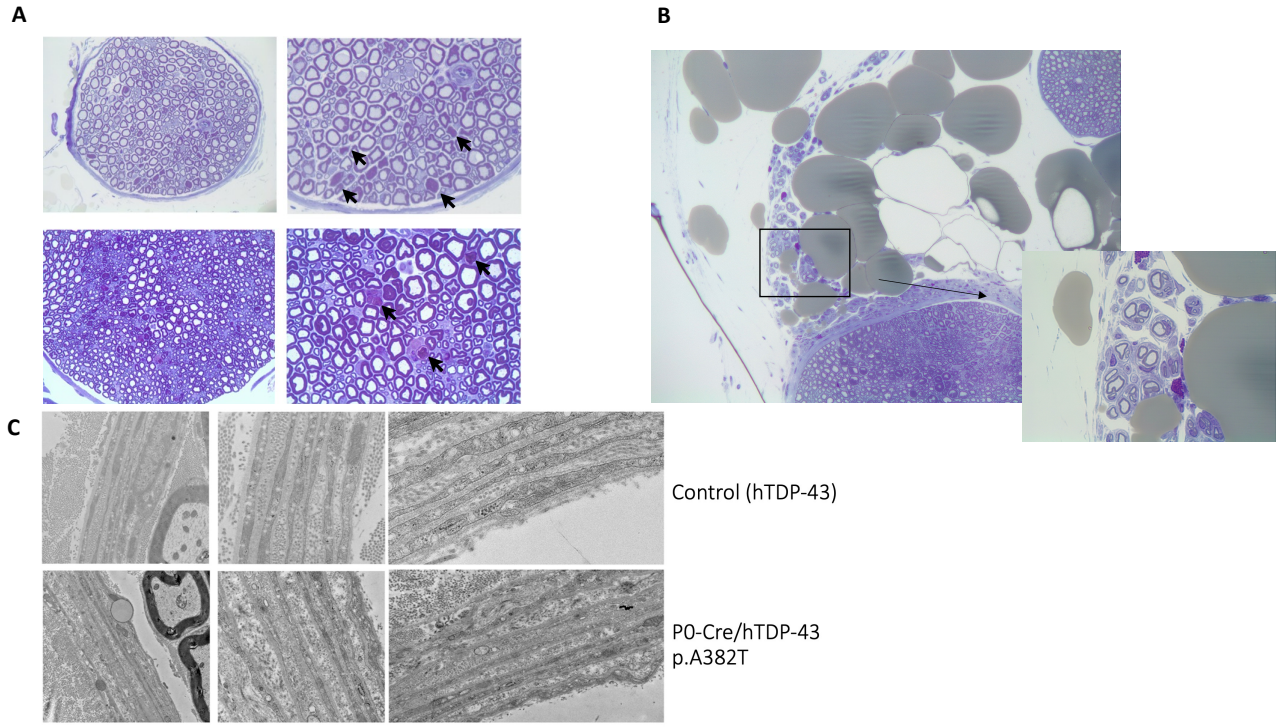

Figure 10: ***Morphological analysis at 18 months.*** *Axonal degenerations in a sciatic nerve section of a P0-Cre/hTDP-43 p.A382T mouse (zoomed in black arrows,* ***A****). Epineural clusters of small fibers are pointed out in sciatic nerve sections of a P0-Cre/hTDP-43 p.A382T mouse in* ***B****. Perineurial cells of P0-Cre/hTDP-43 p.A382T display less transcytosis vesicles compared to control (****C****).*

Molecular characterization of P0-Cre/hTDP-43 mice

Real-time quantitative PCR performed on sciatic nerve lysates from postnatal day 30 mice showed that hTDP-43 transcript expression was detectable in hTDP-43 p.A382T mice and P0-Cre/hTDP-43 p.A382T mice, with significantly higher levels (about a 2-fold difference) in the latter. hTDP-43 transcript was undetectable in WT mice. P0-Cre/hTDP-43 p.A382T mice had higher total (mouse plus human) TDP-43 transcript levels in the sciatic nerve compared to WT mice, by approximately 1.5 – 1.8 folds, whereas total TDP-43 transcript levels were comparable between hTDP-43 p.A382T control mice and WT mice. The increase in total TDP-43 and hTDP-43 transcript was not accompanied by a reduction of endogenous mouse TDP-43. The analysis was repeated at later timepoints, showing similar results. Thus, P0-Cre/hTDP-43 p.A382T mice expressed the transgene in sciatic nerves with a moderate increase of total TDP-43 levels, which was not counteracted by

endogenous TDP-43 autoregulation (Figure 11A). Our transgenic expression system effectively induced hTDP-43 mRNA expression in the sciatic nerve of P0-Cre/hTDP-43 p.A382T mice; hTDP-43 mRNA was detectable also in the sciatic nerves of hTDP-43 p.A382T control mice, not significantly increasing total TDP-43 transcript level.

Similar results were observed when we performed real-time quantitative PCR on sciatic nerves from mice with the hTDP-43 WT transgene. Specifically, hTDP-43 transcript expression was detectable in hTDP-43 WT mice and P0-Cre/hTDP-43 WT mice, with significantly higher levels in P0-Cre/hTDP-43 WT mice. The increase in total TDP-43 and hTDP-43 transcript was not accompanied by a reduction of endogenous mouse TDP-43, comparably to what we observed in mice with the mutated transgene (Figure 11B). Overall, the two constructs (hTDP-43 p.A382T and hTDP-43 WT) induced similar expression levels.

Western blot performed on sciatic nerves at different timepoints using a monoclonal antibody selective for hTDP-43 (60019-2-Ig, Proteintech; (Igaz *et al*, 2011)) did not detect expression at protein level at any timepoint (Figure 11C). Testing with different antibodies reporting human specificity (H00023435 Abnova, LS-B4521, LS-Bio) led to the same results or showed aspecific signal. In order to exclude that the absence of hTDP-43 signal in our transgenic mice was due to solubility issues, being TDP-43 an aggregation-prone protein, we performed Western blot on RIPA-insoluble urea fractions, which did not show hTDP-43 signal. We then performed immunostaining on sciatic nerves using the same set of monoclonal antibodies at different timepoints, which did not demonstrate transgene expression at protein level (Figure 11D). These findings, together, with the absence of endogenous TDP-43 autoregulation, suggest that P0-Cre/hTDP-43 p.A382T mice probably express TDP-43 protein at an extremely low level.

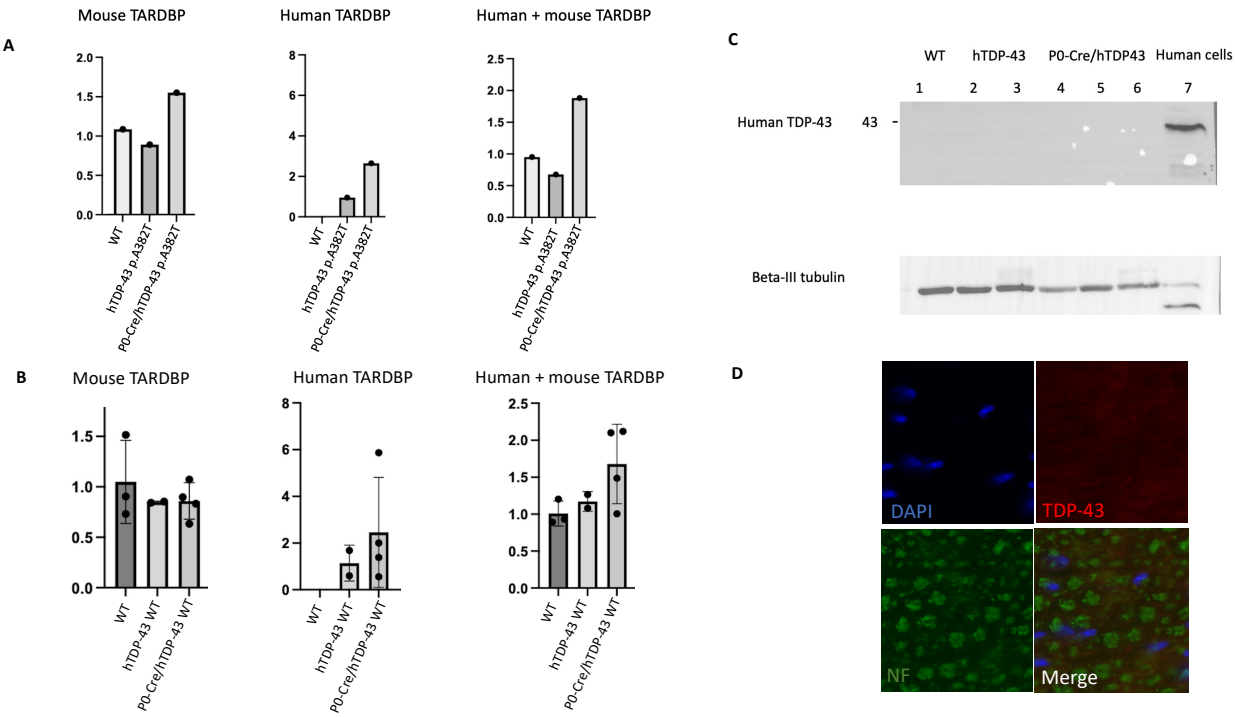

Figure 11: ***Evaluation of transgene expression in sciatic nerves of P0-Cre/hTDP-43 mice.*** *On the left, RT-qPCRs for endogenous mouse TARDBP transcript, human transgenic TARDBP transcript and for total TARDBP transcript in 6-month-old P0-Cre/hTDP-43 p.A382T mice (**A,** the mean value of three samples per genotype is represented) and P0-Cre/hTDP-43 WT mice (**B**); expression was normalized to 18S rRNA. In **C**, Western blot for human TDP-43 protein in the sciatic nerve lysate was performed using a specie-specific antibody (Proteintech, 60019-2-Ig). The experiment shown in the figure was performed on 9-month-old mice. Lane 1: WT mouse. Lanes 2 and 3: control hTDP-43 p.A382T mice. Lanes 4, 5 and 6: P0-Cre/hTDP-43 p.A382T mice. Lane 7: human fibroblast lysate (positive control). The same antibody was used also in immunofluorescence, not showing human TDP-43 specific signal; the experiment shown in **D** was performed on a 9-month-old P0-Cre/hTDP-43 p.A382T mouse. NF: neurofilament.*

We also performed immunostaining for total TDP-43 in sciatic nerves of P0-Cre/hTDP-43 p.A382T mice at different timepoints. Surprisingly, total TDP-43 signal (tested with a non-specie-specific antibody, Proteintech 10782-2-AP) appeared to be increased in P0-Cre/hTDP-43 p.A382T mice compared to controls and localized also in the cytoplasm of SCs (Figure 12A). Interestingly, TDP-43 signal was also sporadically detectable in the nearby axons (Figure 12B). This finding suggests that the low-level expression of transgenic human mutated TDP-43 in SCs might be sufficient to induce detectable alterations in TDP-43 expression and subcellular localization, possibly also affecting the axons.

Since some paranodes of unusual morphology were observed in semithin sections stained with toluidine blue and in TEM (see neuropathological characterization), we investigated by

immunofluorescence the expression and distribution of the main paranodal proteins on teased sciatic nerves. Gliomedin, neurofascin and contactin-associated protein (CASPR) did not differ in signal intensity and distribution between genotypes. However, the nodes of Ranvier, measured as the distance between paranodal CASPR signal, were significantly longer in P0-Cre/hTDP-43 p.A382T mice than in controls (Figure 13A), a finding which was confirmed at electron microscopy analysis. Since TDP-43 has been reported to regulate neurofascin splicing in mouse, we performed a Western blot for neurofascin, which did not show quantitative differences between genotypes.

Despite the absence of an over inflammatory infiltrate, we also tested sciatic nerve lysates for GFAP, a marker of SC activation after damage, by Western blot, which did not show significant differences.

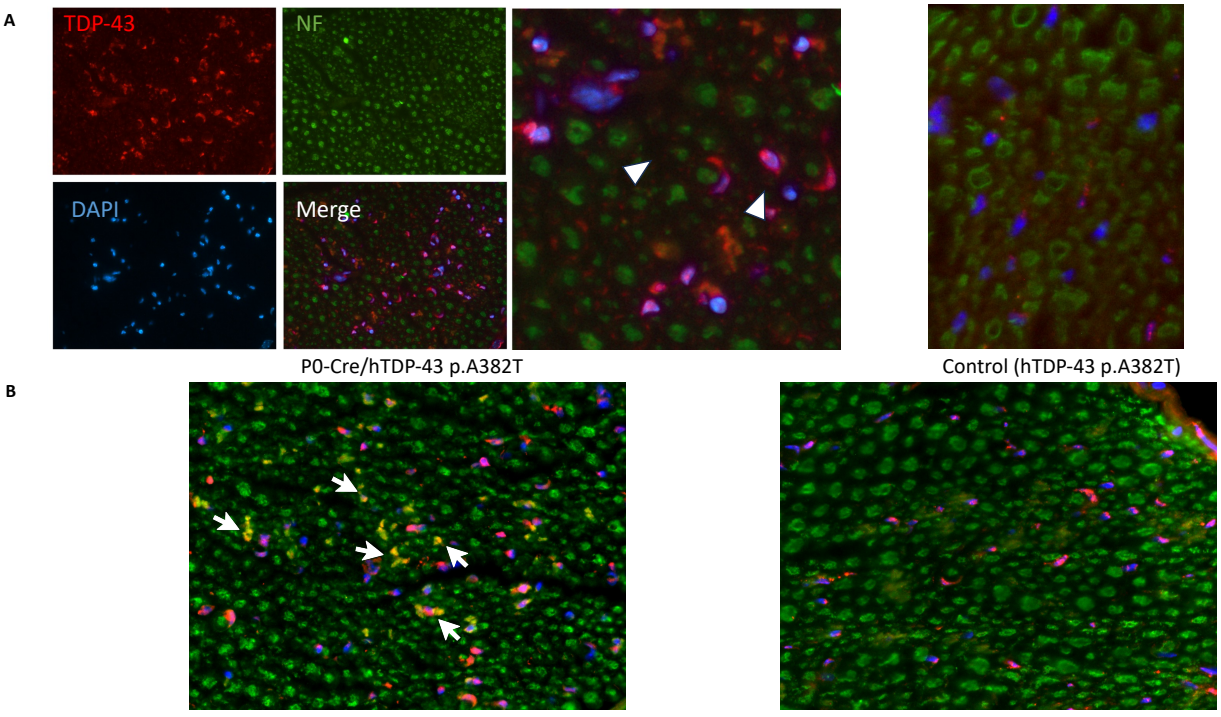

Figure 12: ***TDP-43 mislocalization in sciatic nerves of P0-Cre/hTDP-43 p.A382T mice.*** *Immunofluorescence in sciatic nerves of 9-month-old P0-Cre/hTDP-43 p.A382T mice and littermate controls, using a TDP-43 non-specie specific antibody (Proteintech 10782-2-AP) shows increased signal intensity, with localization to Schwann cell nuclei and cytoplasm (white arrowpoints,* ***A****). In* ***B****, TDP-43 signal co-localizes with neurofilament axonal signal in some axons (white arrows).*

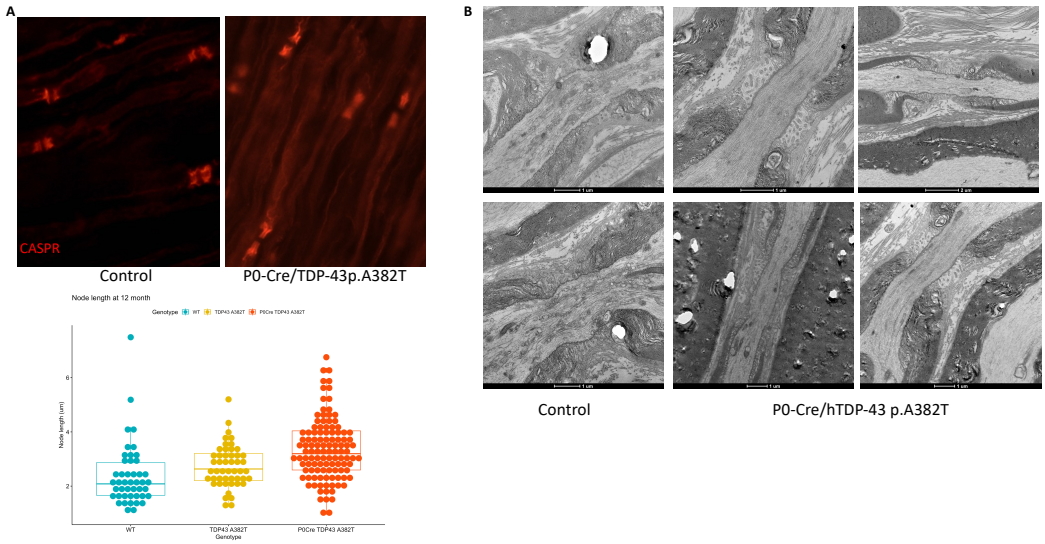

Figure 13: ***P0-Cre/hTDP-43 p.A382T mice have longer nodes of Ranvier.*** *In the left side of the figure* ***(A)****, representative images of an immunofluorescence for the paranodal axonal marker CASPR on teased sciatic nerves from a 12-month-old P0-Cre/hTDP-43 p.A382T mouse and a littermate control show difference in the length of the nodes of Ranvier, with the quantification below (n=7, 2 WT, 2 hTDP-43 p.A382T controls, 3 P0-Cre/hTDP-43 p.A382T; each dot is a node of Ranvier). Increased length of the nodes of Ranvier was confirmed at electron microscopy analysis* ***(B)****.*

Characterization of ChAT-Cre/hTDP-43 mice

ChAT-Cre/hTDP-43 p.A382T and ChAT-Cre/hTDP-43 WT mice were designed in order to separately assess the cell autonomous effect of the transgene expression in spinal motor neurons, by inducing the expression of human TDP-43 in cholinergic neurons. hTDP-43 p.A382T and hTDP-43 WT littermate mice, along with WT littermate mice, were respectively used as controls. ChAT-Cre/hTDP-43 mice underwent the same neurophysiological and behavioral assessments of P0-Cre/hTDP-43 mice. Transgenic mice were vital, were born in the expected mendelian ratio, had a similar weight at birth compared to control and WT mice and were overall phenotypically normal, without showing gross malformations or behavioral abnormalities at birth. RT-qPCR performed on spinal cord lysates detected human TARDBP transcript in ChAT-Cre/hTDP-43 p.A382T mice, and at a lower level in hTDP-43 p.A382T control mice; hTDP-43 transcript was not detectable in WT mice (Figure 14A). We could not directly demonstrate the presence of the human protein by Western blot or immunofluorescence using a human-specific anti TDP-43 monoclonal antibody, similarly to what we observed in P0-Cre/hTDP-43 mice. Motor and mixed nerves (quadriceps and sciatic, respectively) were morphologically normal, without signs of axonal degeneration or differences in myelinated fiber density (Figure 14B). To assess the subcellular localization of TDP-43, we tested the spinal cords and motor nerves by immunofluorescence with a non-specie-specific antibody. We did not observe any difference in signal intensity or spatial distribution between genotypes (Figure 14C).

Immunohistochemistry for ChAT on spinal cord sections did not show apparent motor neuron loss. ChAT-Cre/hTDP-43 p.A382T did not develop any neurophysiological or behavioral phenotype at any timepoints up to 18 months of age (Figure 14D and 14E). ChAT-Cre/hTDP-43 WT mice characterization led to comparable results.

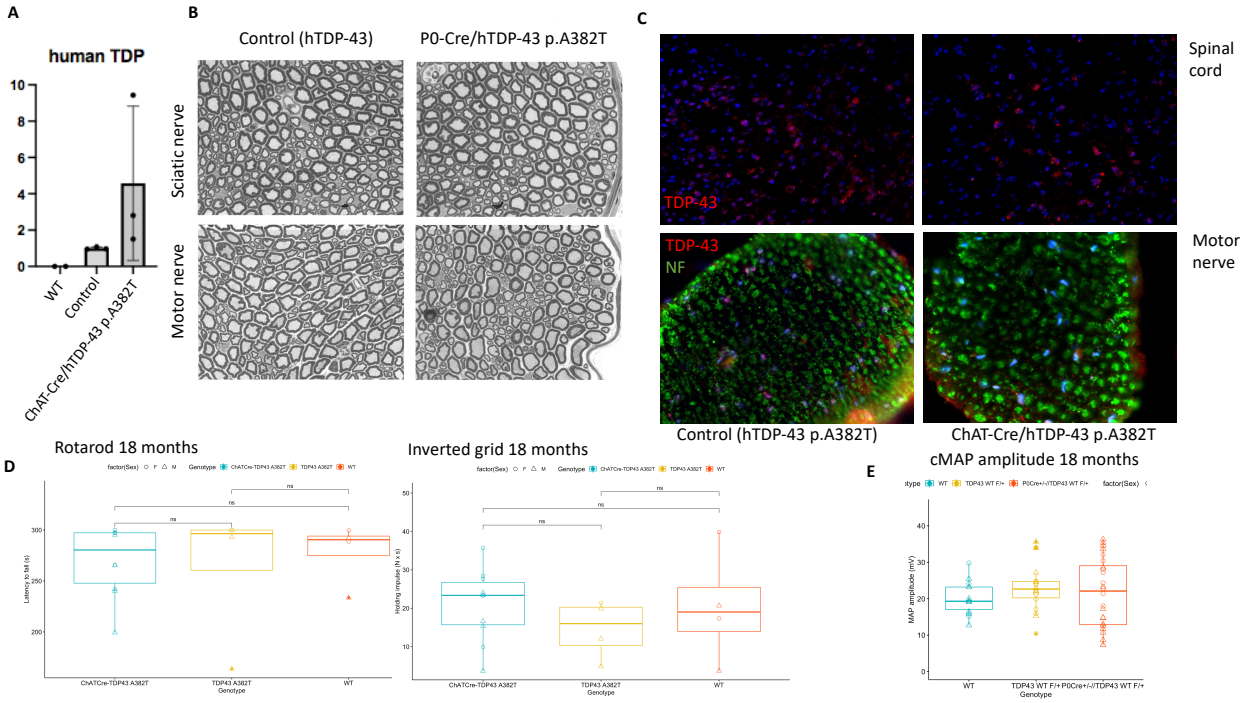

Figure 14: ***Characterization of ChAT-Cre/hTDP-43 mice.*** *In **A**, human TARDBP transcript measured by RT-qPCR in the spinal cord lysate of 6-month-old ChAT-Cre/hTDP-43 p.A382T mice and littermate controls, expression was normalized to rRNA 18S. Sciatic and quadriceps nerves of 9-month-old ChAT-Cre/hTDP-43 p.A382T mice did not show axonal degeneration or fiber loss at morphological evaluation (**B**). We did not observe difference in TDP-43 localization in spinal cord and quadriceps nerve sections stained with a non-specie specific TDP-43 antibody (**C**). ChAT-Cre/hTDP-43 p.A382T mice did not develop behavioral (**D**) or neurophysiological (**E**) alterations.*

Discussion

The aim of this project was to evaluate if the expression of pathological TDP-43 in SCs could contribute to neurodegeneration.

The results obtained from the in vivo model suggest this possibility. Our mouse model is, at the best of our knowledge, the first attempt to induce the SC-selective expression of mutated TDP-43, although a mouse model with SC-selective TDP-43 knockout has already been described(Chang *et al*, 2021).

P0-Cre/hTDP-43 p.A382T and P0-Cre/hTDP-43 WT mice probably express very low level of the transgenic protein, as suggested by the absence of hTDP-43 specific signal on Western blot and the unchanged endogenous TDP-43 transcript level. Our mice did not develop an overt behavioral or neurophysiological phenotype. Survival rate evaluation was not performed in our mice, however after 18 months of observation we observed only few sporadic deaths, without relevant differences among genotypes. P0-Cre/hTDP-43 p.A382T displayed a sparse mild neuropathological phenotype, with myelin and axonal involvement: abnormal myelination, altered paranodes and sporadic axonal degenerations were observed from 9 months of age. The sporadic character of these pathological abnormalities justifies the lack of a neurophysiological phenotype, since a relevant number of myelinated nerve fibers needs to be affected to cause detectable alterations at neurophysiological studies. Immunostaining and Western blot showed differences in quantitative expression and distribution of TDP-43, although we could not discriminate between endogenous and transgenic protein. Importantly, even though our model does not develop a motor phenotype resembling ALS, the neuropathological phenotype appears only in adult age and evolves over time. This model, in consideration of its mild adult-onset phenotype, might represent a platform for the study of environmental stressors and epigenetic factors in TDP-43-related diseases. We have recently generated mice homozygous for human TDP-43 p.A382T, with the aim to detect human TDP-43 at protein level in the model, and we are currently characterizing them.

TDP-43 might be important for axo-glial interactions in mouse SCs. Double myelination figures were reported in a previously described mouse model of TDP-43 cKO in the oligodendrocytes (Heo *et al*, 2022), similar to what we observed in the peripheral nerve of our mouse model. A mouse model of TDP-43 cKO in the SCs showed low motor nerve conduction velocity, linked to splicing alterations involving the transcript of the SC-specific isoform of neurofascin (neurofascin 155), resulting in disruption of the paranodal junctions (Chang *et al*, 2021). In our mouse model, we did not observe alterations in neurofascin protein levels or distribution; however, sporadic abnormalities of the paranodes were evident in toluidine blue-stained sections and electron microscopy. The fact that the expression of transgenic TDP-43 p.A382T resulted in alterations which remind those observed in KO

models is interesting. Importantly, it should be reminded that the observations linked to TDP-43 altered function observe in mouse models are not always translatable to other species, since the binding of TDP-43 to its RNA targets depends on non-conserved sequences. Importantly, we observed a mild pathological phenotype in P0-Cre/hTDP-43 p.A382T mice and not in P0-Cre/hTDP-43 WT mice, suggesting that the alterations are a consequence of the presence of the mutated TDP-43 protein and that the expression of transgenic WT TDP-43 at near-normal is not toxic. This result is in line with the observations from a previous study in which a single copy of the human TDP-43 gene, either mutated or WT, was inserted in the ROSA26 locus; the transgenic protein expression in that case was not restricted to a single cell-type, and the regulatory regions of human TDP-43 were included in the construct (Gordon *et al*, 2019).

Unfortunately, we were unable to observe the cell autonomous effect of TDP-43 p.A382T in our in vivo model, since ChAT-Cre/hTDP-43 mice did not develop any detectable alteration. This is likely due to the fact that motor neurons represent less than 0.5% of the neurons in the spinal cord (Gautier *et al*, 2023). To our knowledge, this was the first attempt to express transgenic TDP-43 selectively in mouse ChAT-positive neurons, whereas conditional knockout mouse models of TDP-43 in the same cell-type has been previously generated and resulted in progressive motor neuron loss (Iguchi *et al*, 2013; Donde *et al*, 2019). The expression of pathological TDP-43 in ChAT-positive neurons did not lead to observable phenotypes; however, we could not define whether this was due to the low level of expression or to other factors. Longer observation and/or a different strategy for transgene expression might be necessary to study the effect of the TARDBP p.A382T mutation in motor neurons.

The results from the in vitro model support the idea that SCs with the TDP-43 p.A382T mutation might exert a toxic non-cell autonomous effect on motor neurons, since TDP-43 WT iMN exhibited a reduction in axonal growth when co-cultured with TDP-43 p.A382T iSCs, compared to when they were co-cultured with TDP-43 WT iSCs. Notably, the presence of the mutation in the iMNs limited itself the axonal growth, as shown by the finding that axonal growth was reduced when TDP-43 p.A382T iMNs were co-cultured with TDP-43 WT iSCs, confirming that the cell autonomous toxicity due to the mutation is detectable in our in vitro model. In a previous study, synaptic abnormalities and abnormal spontaneous activity were reported in iMNs in which the homozygous TDP-43 p.A382T mutation was generated using gene editing (Lépine *et al*, 2024). Comparably to our findings, no changes in TDP-43 total level or distribution were observed; however, axonal branching in monoculture was reported unchanged. Little is known about the effects of the TDP-43 p.A382T mutation at molecular level. The mutation has been reported to impair stress granule formation and alter mitochondrial dynamics in vitro in patient-derived fibroblasts (Orrù *et al*, 2016; Zanini *et al*,

2022). Another study reported a gain of splicing function in primary fibroblasts with this mutation (Fratta *et al*, 2018). In our project, STMN2 exon 2b was detected in iMNs with the TDP-43 p.A382T variant, suggesting loss of TDP-43 function.

To our knowledge, this is the first co-culture ALS-related model including iPSC-derived SCs. Previous compartmentalized models have been used in ALS research to re-create the spatial organization of the motor unit (Osaki *et al*, 2018; Stoklund Dittlau *et al*, 2021). Our model might represent a valuable platform for studying the effect of cell-type specific alterations in the motor unit.

In order to overcome the limitations of our in vivo model, we have generated mice with two copies of the transgene (both inserted in the Rosa26 loci). The goal is to obtain a detectable amount of transgenic protein, and potentially to observe a measurable phenotype. We will also test the expression of TDP-43 RNA targets in the mouse SCs, such as neurofascin, in order to detect whether the expression of disease-associated TDP-43 results in changes at transcript level.

There is no current study evaluating TDP-43 target transcripts in human SCs. TDP-43 targets in other human cell types, such as neurons, have been explored by performing a TDP-43 knockdown and RNA-seq. iPSC-derived immature SCs might provide useful insights to understand which transcripts are controlled by TDP-43 in human SCs, which might then be tested on human nerve biopsies to confirm if TDP-43 dysfunction occurs in ALS patient SCs.

Bibliography

Abramzon YA, Fratta P, Traynor BJ & Chia R (2020) The Overlapping Genetics of Amyotrophic Lateral Sclerosis and Frontotemporal Dementia. *Frontiers in Neuroscience* 14

Agra Almeida Quadros AR, Li Z, Wang X, Ndayambaje IS, Aryal S, Ramesh N, Nolan M, Jayakumar R, Han Y, Stillman H, *et al* (2024) Cryptic splicing of stathmin-2 and UNC13A mRNAs is a pathological hallmark of TDP-43-associated Alzheimer's disease. *Acta Neuropathol* 147: 9

Al-Chalabi A, Fang F, Hanby MF, Leigh PN, Shaw CE, Ye W & Rijsdijk F (2010) An estimate of amyotrophic lateral sclerosis heritability using twin data. *J Neurol Neurosurg Psychiatry* 81: 1324–1326

Alhindi A, Shand M, Smith HL, Leite AS, Huang Y-T, van der Hoorn D, Ridgway Z, Faller KME, Jones RA, Gillingwater TH, *et al* (2023) Neuromuscular junction denervation and terminal Schwann cell loss in the hTDP-43 overexpression mouse model of amyotrophic lateral sclerosis. *Neuropathol Appl Neurobiol* 49: e12925

Armas JMB, Taoro-González L, Fisher EMC & Acevedo-Arozena A (2025) Challenges of modelling TDP-43 pathology in mice. *Mamm Genome* 36: 465–481

Arnold ES, Ling S-C, Huelga SC, Lagier-Tourenne C, Polymenidou M, Ditsworth D, Kordasiewicz HB, McAlonis-Downes M, Platoshyn O, Parone PA, *et al* (2013) ALS-linked TDP-43 mutations produce aberrant RNA splicing and adult-onset motor neuron disease without aggregation or loss of nuclear TDP-43. *Proc Natl Acad Sci U S A* 110: E736-745

Arseni D, Chen R, Murzin AG, Peak-Chew SY, Garringer HJ, Newell KL, Kametani F, Robinson AC, Vidal R, Ghetti B, *et al* (2023) TDP-43 forms amyloid filaments with a distinct fold in type A FTLD-TDP. *Nature* 620: 898–903

Ayala YM, De Conti L, Avendaño-Vázquez SE, Dhir A, Romano M, D'Ambrogio A, Tollervey J, Ule J, Baralle M, Buratti E, *et al* (2011) TDP-43 regulates its mRNA levels through a negative feedback loop. *EMBO J* 30: 277–288

de Boer EMJ, Orie VK, Williams T, Baker MR, De Oliveira HM, Polvikoski T, Silsby M, Menon P, van den Bos M, Halliday GM, *et al* (2020) TDP-43 proteinopathies: a new wave of neurodegenerative diseases. *J Neurol Neurosurg Psychiatry* 92: 86–95

Boillée S, Yamanaka K, Lobsiger CS, Copeland NG, Jenkins NA, Kassiotis G, Kollias G & Cleveland DW (2006) Onset and progression in inherited ALS determined by motor neurons and microglia. *Science* 312: 1389–1392

Braak H, Brettschneider J, Ludolph AC, Lee VM, Trojanowski JQ & Del Tredici K (2013) Amyotrophic lateral sclerosis--a model of corticofugal axonal spread. *Nat Rev Neurol* 9: 708–714

Brettschneider J, Arai K, Del Tredici K, Toledo JB, Robinson JL, Lee EB, Kuwabara S, Shibuya K, Irwin DJ, Fang L, *et al* (2014) TDP-43 pathology and neuronal loss in amyotrophic lateral sclerosis spinal cord. *Acta Neuropathol* 128: 423–437

Brettschneider J, Del Tredici K, Toledo JB, Robinson JL, Irwin DJ, Grossman M, Suh E, Van Deerlin VM, Wood EM, Baek Y, *et al* (2013) Stages of pTDP-43 pathology in amyotrophic lateral sclerosis. *Ann Neurol* 74: 20–38

Brettschneider J, Toledo JB, Van Deerlin VM, Elman L, McCluskey L, Lee VM-Y & Trojanowski JQ (2012) Microglial activation correlates with disease progression and upper motor neuron clinical symptoms in amyotrophic lateral sclerosis. *PLoS One* 7: e39216

Brown A-L, Wilkins OG, Keuss MJ, Hill SE, Zanovello M, Lee WC, Bampton A, Lee FCY, Masino L, Qi YA, *et al* (2022) TDP-43 loss and ALS-risk SNPs drive mis-splicing and depletion of UNC13A. *Nature* 603: 131–137

Brown RH & Al-Chalabi A (2017) Amyotrophic Lateral Sclerosis. *N Engl J Med* 377: 162–172

Buratti E (2018) TDP-43 post-translational modifications in health and disease. *Expert Opin Ther Targets* 22: 279–293

Buratti E & Baralle FE (2001) Characterization and functional implications of the RNA binding

properties of nuclear factor TDP-43, a novel splicing regulator of CFTR exon 9. *J Biol Chem* 276: 36337–36343
Carrasco DI, Bahr BA, Seburn KL & Pinter MJ (2016) Abnormal response of distal Schwann cells to denervation in a mouse model of motor neuron disease. *Exp Neurol* 278: 116–126
de Carvalho M & Swash M (2023) Diagnosis and differential diagnosis of MND/ALS: IFCN handbook chapter. *Clin Neurophysiol Pract* 9: 27–38
Chand KK, Lee KM, Lee JD, Qiu H, Willis EF, Lavidis NA, Hilliard MA & Noakes PG (2018) Defects in synaptic transmission at the neuromuscular junction precede motor deficits in a TDP-43Q331K transgenic mouse model of amyotrophic lateral sclerosis. *FASEB J* 32: 2676–2689
Chang J, Teo AH, Shaw TB, Dupuis L, Ngo ST & Steyn FJ (2025) Deciphering hypothalamic pathology in ALS: insights into non-motor symptoms and disease progression. *eBioMedicine* 118
Chang K-J, Agrawal I, Vainshtein A, Ho WY, Xin W, Tucker-Kellogg G, Susuki K, Peles E, Ling S-C & Chan JR (2021) TDP-43 maximizes nerve conduction velocity by repressing a cryptic exon for paranodal junction assembly in Schwann cells. *Elife* 10: e64456
Chiò A, Borghero G, Pugliatti M, Ticca A, Calvo A, Moglia C, Mutani R, Brunetti M, Ossola I, Marrosu MG, *et al* (2011) Large Proportion of Amyotrophic Lateral Sclerosis Cases in Sardinia Due to a Single Founder Mutation of the TARDBP Gene. *Arch Neurol* 68: 594–598
Chiò A, Mora G, Restagno G, Brunetti M, Ossola I, Barberis M, Ferrucci L, Canosa A, Manera U, Moglia C, *et al* (2013) UNC13A influences survival in Italian amyotrophic lateral sclerosis patients: a population-based study. *Neurobiol Aging* 34: 357.e1–5
Colombrita C, Zennaro E, Fallini C, Weber M, Sommacal A, Buratti E, Silani V & Ratti A (2009) TDP-43 is recruited to stress granules in conditions of oxidative insult. *J Neurochem* 111: 1051–1061
Coyne AN, Zaepfel BL, Hayes L, Fitchman B, Salzberg Y, Luo E-C, Bowen K, Trost H, Aigner S, Rigo F, *et al* (2020) G4C2 Repeat RNA Initiates a POM121-Mediated Reduction in Specific Nucleoporins in C9orf72 ALS/FTD. *Neuron* 107: 1124-1140.e11
Cykowski MD, Powell SZ, Appel JW, Arumanayagam AS, Rivera AL & Appel SH (2018) Phosphorylated TDP-43 (pTDP-43) aggregates in the axial skeletal muscle of patients with sporadic and familial amyotrophic lateral sclerosis. *Acta Neuropathologica Communications* 6: 28
De Vitis E, La Pesa V, Gervaso F, Romano A, Quattrini A, Gigli G, Moroni L & Polini A (2021) A microfabricated multi-compartment device for neuron and Schwann cell differentiation. *Sci Rep* 11: 7019
Ditsworth D, Maldonado M, McAlonis-Downes M, Sun S, Seelman A, Drenner K, Arnold E, Ling S-C, Pizzo D, Ravits J, *et al* (2017) Mutant TDP-43 within motor neurons drives disease onset but not progression in amyotrophic lateral sclerosis. *Acta Neuropathol* 133: 907–922
Dols-Icardo O, Montal V, Sirisi S, López-Pernas G, Cervera-Carles L, Querol-Vilaseca M, Muñoz L, Belbin O, Alcolea D, Molina-Porcel L, *et al* (2020) Motor cortex transcriptome reveals microglial key events in amyotrophic lateral sclerosis. *Neurol Neuroimmunol Neuroinflamm* 7: e829
Donde A, Sun M, Ling JP, Braunstein KE, Pang B, Wen X, Cheng X, Chen L & Wong PC (2019) Splicing Repression is a Major Function of TDP-43 in Motor Neurons. *Acta Neuropathol* 138: 813–826
Du Z-W, Chen H, Liu H, Lu J, Qian K, Huang C-L, Zhong X, Fan F & Zhang S-C (2015) Generation and expansion of highly pure motor neuron progenitors from human pluripotent stem cells. *Nat Commun* 6: 6626
Duan L, Zaepfel BL, Aksenova V, Dasso M, Rothstein JD, Kalab P & Hayes LR (2022) Nuclear RNA binding regulates TDP-43 nuclear localization and passive nuclear export. *Cell Rep* 40: 111106
van Es MA, Hardiman O, Chio A, Al-Chalabi A, Pasterkamp RJ, Veldink JH & van den Berg LH (2017) Amyotrophic lateral sclerosis. *Lancet* 390: 2084–2098
Fehmi J, Scherer SS, Willison HJ & Rinaldi S (2018) Nodes, paranodes and neuropathies. *J Neurol*

Neurosurg Psychiatry 89: 61–71
Feldman EL, Goutman SA, Petri S, Mazzini L, Savelieff MG, Shaw PJ & Sobue G (2022) Amyotrophic lateral sclerosis. *Lancet* 400: 1363–1380
Feltri ML, D'Antonio M, Previtali S, Fasolini M, Messing A & Wrabetz L (1999) P0-Cre transgenic mice for inactivation of adhesion molecules in Schwann cells. *Ann N Y Acad Sci* 883: 116–123
Feltri ML, Poitelon Y & Previtali SC (2016) How Schwann Cells Sort Axons: New Concepts. *Neuroscientist* 22: 252–265
Fernandopulle MS, Prestil R, Grunseich C, Wang C, Gan L & Ward ME (2018) Transcription Factor-Mediated Differentiation of Human iPSCs into Neurons. *Curr Protoc Cell Biol* 79: e51
Ferraiuolo L, Meyer K, Sherwood TW, Vick J, Likhite S, Frakes A, Miranda CJ, Braun L, Heath PR, Pineda R, *et al* (2016) Oligodendrocytes contribute to motor neuron death in ALS via SOD1-dependent mechanism. *Proc Natl Acad Sci U S A* 113: E6496–E6505
Fischer LR, Culver DG, Tennant P, Davis AA, Wang M, Castellano-Sanchez A, Khan J, Polak MA & Glass JD (2004) Amyotrophic lateral sclerosis is a distal axonopathy: evidence in mice and man. *Exp Neurol* 185: 232–240
Fratta P, Sivakumar P, Humphrey J, Lo K, Ricketts T, Oliveira H, Brito-Armas JM, Kalmar B, Ule A, Yu Y, *et al* (2018) Mice with endogenous TDP-43 mutations exhibit gain of splicing function and characteristics of amyotrophic lateral sclerosis. *EMBO J* 37: e98684
Fridman V & Saporta MA (2021) Mechanisms and Treatments in Demyelinating CMT. *Neurotherapeutics* 18: 2236–2268
Gautier O, Blum JA, Maksymetz J, Chen D, Schweingruber C, Mei I, Hermann A, Hackos DH, Hedlund E, Ravits J, *et al* (2023) Challenges of profiling motor neuron transcriptomes from human spinal cord. *Neuron* 111: 3739–3741
Gendron TF, Chew J, Stankowski JN, Hayes LR, Zhang Y-J, Prudencio M, Carlomagno Y, Daughrity LM, Jansen-West K, Perkerson EA, *et al* (2017) Poly(GP) proteins are a useful pharmacodynamic marker for C9ORF72-associated amyotrophic lateral sclerosis. *Sci Transl Med* 9: eaai7866
Ghidinelli M, Poitelon Y, Shin YK, Ameroso D, Williamson C, Ferri C, Pellegatta M, Espino K, Mogha A, Monk K, *et al* (2017) Laminin 211 inhibits protein kinase A in Schwann cells to modulate neuregulin 1 type III-driven myelination. *PLoS Biol* 15: e2001408
Godoy-Corchuelo JM, Ali Z, Brito Armas JM, Martins-Bach AB, García-Toledo I, Fernández-Beltrán LC, López-Carbonero JI, Bascuñana P, Spring S, Jimenez-Coca I, *et al* (2024) TDP-43-M323K causes abnormal brain development and progressive cognitive and motor deficits associated with mislocalised and increased levels of TDP-43. *Neurobiol Dis* 193: 106437
Gordon D, Dafinca R, Scaber J, Alegre-Abarrategui J, Farrimond L, Scott C, Biggs D, Kent L, Oliver PL, Davies B, *et al* (2019) Single-copy expression of an amyotrophic lateral sclerosis-linked TDP-43 mutation (M337V) in BAC transgenic mice leads to altered stress granule dynamics and progressive motor dysfunction. *Neurobiol Dis* 121: 148–162
Gould TW, Ko C-P, Willison H & Robitaille R (2025) Perisynaptic Schwann Cells: Guardians of Neuromuscular Junction Integrity and Function in Health and Disease. *Cold Spring Harb Perspect Biol* 17: a041362
Greenfield S, Brostoff S, Eylar EH & Morell P (1973) Protein composition of myelin of the peripheral nervous system. *J Neurochem* 20: 1207–1216
Guillén-Boixet J, Kopach A, Holehouse AS, Wittmann S, Jahnel M, Schlüßler R, Kim K, Trussina IREA, Wang J, Mateju D, *et al* (2020) RNA-Induced Conformational Switching and Clustering of G3BP Drive Stress Granule Assembly by Condensation. *Cell* 181: 346-361.e17
Guillot SJ, Lang C, Simonot M, Beckett D, Lulé D, Balz LT, Knehr A, Stuart-Lopez G, Vercruysse P, Dieterlé S, *et al* (2025) Early-onset sleep alterations found in patients with amyotrophic lateral sclerosis are ameliorated by orexin antagonist in mouse models. *Science Translational Medicine* 17: eadm7580

Haidet-Phillips AM, Hester ME, Miranda CJ, Meyer K, Braun L, Frakes A, Song S, Likhite S, Murtha MJ, Foust KD, *et al* (2011) Astrocytes from familial and sporadic ALS patients are toxic to motor neurons. *Nat Biotechnol* 29: 824–828
Hardiman O, Al-Chalabi A, Chio A, Corr EM, Logroscino G, Robberecht W, Shaw PJ, Simmons Z & van den Berg LH (2017) Amyotrophic lateral sclerosis. *Nat Rev Dis Primers* 3: 17071
Harrison JM & Rafuse VF (2020) Muscle fiber-type specific terminal Schwann cell pathology leads to sprouting deficits following partial denervation in SOD1G93A mice. *Neurobiol Dis* 145: 105052
Heads T, Pollock M, Robertson A, Sutherland WHF & Allpress S (1991) Sensory nerve pathology in amyotrophic lateral sclerosis. *Acta Neuropathol* 82: 316–320
Heo D, Ling JP, Molina-Castro GC, Langseth AJ, Waisman A, Nave K-A, Möbius W, Wong PC & Bergles DE (2022) Stage-specific control of oligodendrocyte survival and morphogenesis by TDP-43. *Elife* 11: e75230
Hirasawa Y, Saiki T, Nakao Y & Katsumi Y (1994) Regeneration of perineurium after nerve injury and autografting. An experimental study. *Int Orthop* 18: 229–235
Hörner SJ, Couturier N, Gueiber DC, Hafner M & Rudolf R (2022) Development and In Vitro Differentiation of Schwann Cells. *Cells* 11: 3753
Igaz LM, Kwong LK, Lee EB, Chen-Plotkin A, Swanson E, Unger T, Malunda J, Xu Y, Winton MJ, Trojanowski JQ, *et al* (2011) Dysregulation of the ALS-associated gene TDP-43 leads to neuronal death and degeneration in mice. *J Clin Invest* 121: 726–738
Iguchi Y, Katsuno M, Niwa J, Takagi S, Ishigaki S, Ikenaka K, Kawai K, Watanabe H, Yamanaka K, Takahashi R, *et al* (2013) Loss of TDP-43 causes age-dependent progressive motor neuron degeneration. *Brain* 136: 1371–1382
Iwanaga T, Takahashi-Iwanaga H, Nio-Kobayashi J & Ebara S (2022) Structure and barrier functions of the perineurium and its relationship with associated sensory corpuscles: A review. *Biomed Res* 43: 145–159
Janssens J, Wils H, Kleinberger G, Joris G, Cuijt I, Ceuterick-de Groote C, Van Broeckhoven C & Kumar-Singh S (2013) Overexpression of ALS-associated p.M337V human TDP-43 in mice worsens disease features compared to wild-type human TDP-43 mice. *Mol Neurobiol* 48: 22–35
Jessen KR & Mirsky R (2016) The repair Schwann cell and its function in regenerating nerves. *J Physiol* 594: 3521–3531
Jessen KR, Mirsky R & Lloyd AC (2015) Schwann Cells: Development and Role in Nerve Repair. *Cold Spring Harb Perspect Biol* 7: a020487
Jo M, Lee S, Jeon Y-M, Kim S, Kwon Y & Kim H-J (2020) The role of TDP-43 propagation in neurodegenerative diseases: integrating insights from clinical and experimental studies. *Exp Mol Med* 52: 1652–1662
Kim H-S, Lee J, Lee DY, Kim Y-D, Kim JY, Lim HJ, Lim S & Cho YS (2017) Schwann Cell Precursors from Human Pluripotent Stem Cells as a Potential Therapeutic Target for Myelin Repair. *Stem Cell Reports* 8: 1714–1726
Klim JR, Williams LA, Limone F, Guerra San Juan I, Davis-Dusenbery BN, Mordes DA, Burberry A, Steinbaugh MJ, Gamage KK, Kirchner R, *et al* (2019) ALS-implicated protein TDP-43 sustains levels of STMN2, a mediator of motor neuron growth and repair. *Nat Neurosci* 22: 167–179
Kurashige T, Morino H, Murao T, Izumi Y, Sugiura T, Kuraoka K, Kawakami H, Torii T & Maruyama H (2022) TDP-43 Accumulation Within Intramuscular Nerve Bundles of Patients With Amyotrophic Lateral Sclerosis. *JAMA Neurol* 79: 693–701
Kwiatkowski TJ, Bosco DA, Leclerc AL, Tamrazian E, Vanderburg CR, Russ C, Davis A, Gilchrist J, Kasarskis EJ, Munsat T, *et al* (2009) Mutations in the FUS/TLS gene on chromosome 16 cause familial amyotrophic lateral sclerosis. *Science* 323: 1205–1208
Laferrière F, Maniecka Z, Pérez-Berlanga M, Hruska-Plochan M, Gilhespy L, Hock E-M, Wagner U, Afroz T, Boersema PJ, Barmettler G, *et al* (2019) TDP-43 extracted from frontotemporal lobar degeneration subject brains displays distinct aggregate assemblies and neurotoxic effects reflecting disease progression rates. *Nat Neurosci* 22: 65–77

Lépine S, Nauleau-Javaudin A, Deneault E, Chen CX-Q, Abdian N, Franco-Flores AK, Haghi G, Castellanos-Montiel MJ, Maussion G, Chaineau M, *et al* (2024) Homozygous ALS-linked mutations in TARDBP/TDP-43 lead to hypoactivity and synaptic abnormalities in human iPSC-derived motor neurons. *iScience* 27: 109166
Licht-Murava A, Meadows SM, Palaguachi F, Song SC, Jackvony S, Bram Y, Zhou C, Schwartz RE, Froemke RC, Orr AL, *et al* (2023) Astrocytic TDP-43 dysregulation impairs memory by modulating antiviral pathways and interferon-inducible chemokines. *Sci Adv* 9: eade1282
Ling JP, Pletnikova O, Troncoso JC & Wong PC (2015) TDP-43 repression of nonconserved cryptic exons is compromised in ALS-FTD. *Science* 349: 650–655
Lorente Pons A, Higginbottom A, Cooper-Knock J, Alrafiah A, Alofi E, Kirby J, Shaw PJ, Wood JD & Highley JR (2020) Oligodendrocyte pathology exceeds axonal pathology in white matter in human amyotrophic lateral sclerosis. *J Pathol* 251: 262–271
Ma XR, Prudencio M, Koike Y, Vatsavayai SC, Kim G, Harbinski F, Briner A, Rodriguez CM, Guo C, Akiyama T, *et al* (2022) TDP-43 represses cryptic exon inclusion in the FTD-ALS gene UNC13A. *Nature* 603: 124–130
Mackenzie IRA, Bigio EH, Ince PG, Geser F, Neumann M, Cairns NJ, Kwong LK, Forman MS, Ravits J, Stewart H, *et al* (2007) Pathological TDP-43 distinguishes sporadic amyotrophic lateral sclerosis from amyotrophic lateral sclerosis with SOD1 mutations. *Ann Neurol* 61: 427–434
Malong L, Napoli I, Casal G, White IJ, Stierli S, Vaughan A, Cattin A-L, Burden JJ, Hng KI, Bossio A, *et al* (2023) Characterization of the structure and control of the blood-nerve barrier identifies avenues for therapeutic delivery. *Dev Cell* 58: 174-191.e8
Martineau É, Arbour D, Vallée J & Robitaille R (2020) Properties of Glial Cell at the Neuromuscular Junction Are Incompatible with Synaptic Repair in the SOD1G37R ALS Mouse Model. *J Neurosci* 40: 7759–7777
Mathis S, Goizet C, Soulages A, Vallat J-M & Masson GL (2019) Genetics of amyotrophic lateral sclerosis: A review. *J Neurol Sci* 399: 217–226
Mazzara PG, Massimino L, Pellegatta M, Ronchi G, Ricca A, Iannielli A, Giannelli SG, Cursi M, Cancellieri C, Sessa A, *et al* (2017) Two factor-based reprogramming of rodent and human fibroblasts into Schwann cells. *Nat Commun* 8: 14088
Mead RJ, Shan N, Reiser HJ, Marshall F & Shaw PJ (2023) Amyotrophic lateral sclerosis: a neurodegenerative disorder poised for successful therapeutic translation. *Nat Rev Drug Discov* 22: 185–212
Mejzini R, Flynn LL, Pitout IL, Fletcher S, Wilton SD & Akkari PA (2019) ALS Genetics, Mechanisms, and Therapeutics: Where Are We Now? *Frontiers in Neuroscience* 13
Melamed Z, López-Erauskin J, Baughn MW, Zhang O, Drenner K, Sun Y, Freyermuth F, McMahon MA, Beccari MS, Artates JW, *et al* (2019) Premature polyadenylation-mediated loss of stathmin-2 is a hallmark of TDP-43-dependent neurodegeneration. *Nat Neurosci* 22: 180–190
Moss KR, Bopp TS, Johnson AE & Höke A (2021) New evidence for secondary axonal degeneration in demyelinating neuropathies. *Neurosci Lett* 744: 135595
Nakamura-Shindo K, Sakai K, Shimizu A, Ishida C & Yamada M (2020) Accumulation of phosphorylated TDP-43 in the cytoplasm of Schwann cells in a case of sporadic amyotrophic lateral sclerosis. *Neuropathology* 40: 606–610
Negro S, Pirazzini M & Rigoni M (2022) Models and methods to study Schwann cells. *Journal of Anatomy* 241: 1235–1258
Neumann M, Kwong LK, Truax AC, Vanmassenhove B, Kretzschmar HA, Van Deerlin VM, Clark CM, Grossman M, Miller BL, Trojanowski JQ, *et al* (2007) TDP-43-positive white matter pathology in frontotemporal lobar degeneration with ubiquitin-positive inclusions. *J Neuropathol Exp Neurol* 66: 177–183
Neumann M, Lee EB & Mackenzie IR (2021) Frontotemporal Lobar Degeneration TDP-43-Immunoreactive Pathological Subtypes: Clinical and Mechanistic Significance. *Adv Exp Med Biol* 1281: 201–217

Neumann M, Sampathu DM, Kwong LK, Truax AC, Micsenyi MC, Chou TT, Bruce J, Schuck T, Grossman M, Clark CM, *et al* (2006) Ubiquitinated TDP-43 in frontotemporal lobar degeneration and amyotrophic lateral sclerosis. *Science* 314: 130–133
Nguyen TB, Miramontes R, Chillon-Marinas C, Maimon R, Vazquez-Sanchez S, Lau AL, McClure NR, Wu Z, Wang KQ, England WE, *et al* (2025) Aberrant splicing in Huntington's disease accompanies disrupted TDP-43 activity and altered m6A RNA modification. *Nat Neurosci* 28: 280–292
Nijs M & Van Damme P (2024) The genetics of amyotrophic lateral sclerosis. *Curr Opin Neurol* 37: 560–569
Nishihira Y, Tan C-F, Onodera O, Toyoshima Y, Yamada M, Morita T, Nishizawa M, Kakita A & Takahashi H (2008) Sporadic amyotrophic lateral sclerosis: two pathological patterns shown by analysis of distribution of TDP-43-immunoreactive neuronal and glial cytoplasmic inclusions. *Acta Neuropathol* 116: 169–182
Nolano M, Provitera V, Caporaso G, Fasolino I, Borreca I, Stancanelli A, Iuzzolino VV, Senerchia G, Vitale F, Tozza S, *et al* (2024) Skin innervation across amyotrophic lateral sclerosis clinical stages: new prognostic biomarkers. *Brain* 147: 1740–1750
Nonaka T, Masuda-Suzukake M, Arai T, Hasegawa Y, Akatsu H, Obi T, Yoshida M, Murayama S, Mann DMA, Akiyama H, *et al* (2013) Prion-like properties of pathological TDP-43 aggregates from diseased brains. *Cell Rep* 4: 124–134
Orrù S, Coni P, Floris A, Littera R, Carcassi C, Sogos V & Brancia C (2016) Reduced stress granule formation and cell death in fibroblasts with the A382T mutation of TARDBP gene: evidence for loss of TDP-43 nuclear function. *Hum Mol Genet* 25: 4473–4483
Osaki T, Uzel SGM & Kamm RD (2018) Microphysiological 3D model of amyotrophic lateral sclerosis (ALS) from human iPS-derived muscle cells and optogenetic motor neurons. *Science Advances* 4: eaat5847
Peltonen S, Alanne M & Peltonen J (2013) Barriers of the peripheral nerve. *Tissue Barriers* 1: e24956
Peng AYT, Agrawal I, Ho WY, Yen Y-C, Pinter AJ, Liu J, Phua QXC, Koh KB, Chang J-C, Sanford E, *et al* (2020) Loss of TDP-43 in astrocytes leads to motor deficits by triggering A1-like reactive phenotype and triglial dysfunction. *Proc Natl Acad Sci U S A* 117: 29101–29112
Piña-Oviedo S & Ortiz-Hidalgo C (2008) The normal and neoplastic perineurium: a review. *Adv Anat Pathol* 15: 147–164
Piol D, Robberechts T & Da Cruz S (2023) Lost in local translation: TDP-43 and FUS in axonal/neuromuscular junction maintenance and dysregulation in amyotrophic lateral sclerosis. *Neuron* 111: 1355–1380
Polymenidou M, Lagier-Tourenne C, Hutt KR, Huelga SC, Moran J, Liang TY, Ling S-C, Sun E, Wancewicz E, Mazur C, *et al* (2011) Long pre-mRNA depletion and RNA missplicing contribute to neuronal vulnerability from loss of TDP-43. *Nat Neurosci* 14: 459–468
Rasband MN & Peles E (2016) The Nodes of Ranvier: Molecular Assembly and Maintenance. *Cold Spring Harb Perspect Biol* 8: a020495
Renton AE, Majounie E, Waite A, Simón-Sánchez J, Rollinson S, Gibbs JR, Schymick JC, Laaksovirta H, van Swieten JC, Myllykangas L, *et al* (2011) A hexanucleotide repeat expansion in C9ORF72 is the cause of chromosome 9p21-linked ALS-FTD. *Neuron* 72: 257–268
Riva N, Gentile F, Cerri F, Gallia F, Podini P, Dina G, Falzone YM, Fazio R, Lunetta C, Calvo A, *et al* (2022) Phosphorylated TDP-43 aggregates in peripheral motor nerves of patients with amyotrophic lateral sclerosis. *Brain* 145: 276–284
Rosen DR, Siddique T, Patterson D, Figlewicz DA, Sapp P, Hentati A, Donaldson D, Goto J, O'Regan JP & Deng HX (1993) Mutations in Cu/Zn superoxide dismutase gene are associated with familial amyotrophic lateral sclerosis. *Nature* 362: 59–62
Ruf WP, Boros M, Freischmidt A, Brenner D, Grozdanov V, de Meirelles J, Meyer T, Grehl T, Petri S, Grosskreutz J, *et al* (2023) Spectrum and frequency of genetic variants in sporadic

amyotrophic lateral sclerosis. *Brain Commun* 5: fcad152
Salzer JL (2015) Schwann Cell Myelination. *Cold Spring Harb Perspect Biol* 7: a020529
Scherer SS & Wrabetz L (2008) Molecular mechanisms of inherited demyelinating neuropathies. *Glia* 56: 1578–1589
Schito P, Ceccardi G, Calvo A, Falzone YM, Moglia C, Lunetta C, Marinou K, Ticozzi N, Scialo C, Sorarù G, *et al* (2020) Clinical features and outcomes of the flail arm and flail leg and pure lower motor neuron MND variants: a multicentre Italian study. *J Neurol Neurosurg Psychiatry* 91: 1001–1003
Schumacher N, Vandenbosch R & Franzen R (2025) Peripheral myelin: From development to maintenance. *J Neurochem* 169: e16268
Scialò C, Zhong W, Jagannath S, Wilkins O, Caredio D, Hruska-Plochan M, Lurati F, Peter M, Cecco ED, Celauro L, *et al* (2025) Seeded aggregation of TDP-43 induces its loss of function and reveals early pathological signatures. *Neuron* 113: 1614-1628.e11
Seelaar H, Schelhaas HJ, Azmani A, Küsters B, Rosso S, Majoor-Krakauer D, de Rijk MC, Rizzu P, ten Brummelhuis M, van Doorn PA, *et al* (2007) TDP-43 pathology in familial frontotemporal dementia and motor neuron disease without Progranulin mutations. *Brain* 130: 1375–1385
Sephton CF, Good SK, Atkin S, Dewey CM, Mayer P, Herz J & Yu G (2010) TDP-43 is a developmentally regulated protein essential for early embryonic development. *J Biol Chem* 285: 6826–6834
Serio A, Bilican B, Barmada SJ, Ando DM, Zhao C, Siller R, Burr K, Haghi G, Story D, Nishimura AL, *et al* (2013) Astrocyte pathology and the absence of non-cell autonomy in an induced pluripotent stem cell model of TDP-43 proteinopathy. *Proc Natl Acad Sci U S A* 110: 4697–4702
Sobue G, Matsuoka Y, Mukai E, Takayanagi T & Sobue I (1981) Pathology of myelinated fibers in cervical and lumbar ventral spinal roots in amyotrophic lateral sclerosis. *J Neurol Sci* 50: 413–421
Son Y-J & Thompson WJ (1995) Nerve sprouting in muscle is induced and guided by processes extended by schwann cells. *Neuron* 14: 133–141
Soriano P (1999) Generalized lacZ expression with the ROSA26 Cre reporter strain. *Nat Genet* 21: 70–71
Spiller KJ, Restrepo CR, Khan T, Dominique MA, Fang TC, Canter RG, Roberts CJ, Miller KR, Ransohoff RM, Trojanowski JQ, *et al* (2018) Microglia-mediated recovery from ALS-relevant motor neuron degeneration in a mouse model of TDP-43 proteinopathy. *Nat Neurosci* 21: 329–340
Stewart JD (2003) Peripheral nerve fascicles: Anatomy and clinical relevance. *Muscle & Nerve* 28: 525–541
Stoklund Dittlau K, Krasnow EN, Fumagalli L, Vandoorne T, Baatsen P, Kerstens A, Giacomazzi G, Pavie B, Rossaert E, Beckers J, *et al* (2021) Human motor units in microfluidic devices are impaired by *FUS* mutations and improved by HDAC6 inhibition. *Stem Cell Reports* 16: 2213–2227
Strong MJ, Abrahams S, Goldstein LH, Woolley S, Mclaughlin P, Snowden J, Mioshi E, Roberts-South A, Benatar M, Hortobágyi T, *et al* (2017) Amyotrophic lateral sclerosis - frontotemporal spectrum disorder (ALS-FTSD): Revised diagnostic criteria. *Amyotroph Lateral Scler Frontotemporal Degener* 18: 153–174
Šušnjar U, Škrabar N, Brown A-L, Abbassi Y, Phatnani H, Cortese A, Cereda C, Bugiardini E, Cardani R, Meola G, *et al* (2022) Cell environment shapes TDP-43 function with implications in neuronal and muscle disease. *Commun Biol* 5: 314
Talbott EO, Malek AM & Lacomis D (2016) The epidemiology of amyotrophic lateral sclerosis. *Handb Clin Neurol* 138: 225–238
Taveggia C, Zanazzi G, Petrylak A, Yano H, Rosenbluth J, Einheber S, Xu X, Esper RM, Loeb JA, Shrager P, *et al* (2005) Neuregulin-1 type III determines the ensheathment fate of axons. *Neuron* 47: 681–694
Tollervey JR, Curk T, Rogelj B, Briese M, Cereda M, Kayikci M, König J, Hortobágyi T, Nishimura AL, Župunski V, *et al* (2011) Characterizing the RNA targets and position-dependent splicing regulation by TDP-43. *Nat Neurosci* 14: 452–458

Tondo G, Iaccarino L, Cerami C, Vanoli GE, Presotto L, Masiello V, Coliva A, Salvi F, Bartolomei I, Mosca L, *et al* (2020) 11 C-PK11195 PET-based molecular study of microglia activation in SOD1 amyotrophic lateral sclerosis. *Ann Clin Transl Neurol* 7: 1513–1523
Tong J, Huang C, Bi F, Wu Q, Huang B, Liu X, Li F, Zhou H & Xia X-G (2013) Expression of ALS-linked TDP-43 mutant in astrocytes causes non-cell-autonomous motor neuron death in rats. *EMBO J* 32: 1917–1926
Topilko P, Schneider-Maunoury S, Levi G, Baron-Van Evercooren A, Chennoufi ABY, Seitanidou T, Babinet C & Charnay P (1994) Krox-20 controls myelination in the peripheral nervous system. *Nature* 371: 796–799
Tsai K-J, Yang C-H, Fang Y-H, Cho K-H, Chien W-L, Wang W-T, Wu T-W, Lin C-P, Fu W-M & Shen C-KJ (2010) Elevated expression of TDP-43 in the forebrain of mice is sufficient to cause neurological and pathological phenotypes mimicking FTLD-U. *J Exp Med* 207: 1661–1673
Turner MR, Cagnin A, Turkheimer FE, Miller CCJ, Shaw CE, Brooks DJ, Leigh PN & Banati RB (2004) Evidence of widespread cerebral microglial activation in amyotrophic lateral sclerosis: an [11C](R)-PK11195 positron emission tomography study. *Neurobiol Dis* 15: 601–609
Walker AK, Spiller KJ, Ge G, Zheng A, Xu Y, Zhou M, Tripathy K, Kwong LK, Trojanowski JQ & Lee VM-Y (2015) Functional recovery in new mouse models of ALS/FTLD after clearance of pathological cytoplasmic TDP-43. *Acta Neuropathol* 130: 643–660
Wang J, Ho WY, Lim K, Feng J, Tucker-Kellogg G, Nave K-A & Ling S-C (2018) Cell-autonomous requirement of TDP-43, an ALS/FTD signature protein, for oligodendrocyte survival and myelination. *Proc Natl Acad Sci U S A* 115: E10941–E10950
Wiedemann C (2010) Schwann cells roll the dice. *Nat Rev Neurosci* 11: 457–457
Wilson ER, Della-Flora Nunes G, Weaver MR, Frick LR & Feltri ML (2021) Schwann cell interactions during the development of the peripheral nervous system. *Dev Neurobiol* 81: 464–489
Xie M, Zhao S, Bosco DB, Nguyen A & Wu L-J (2022) Microglial TREM2 in amyotrophic lateral sclerosis. *Dev Neurobiol* 82: 125–137
Yamanaka K, Chun SJ, Boillee S, Fujimori-Tonou N, Yamashita H, Gutmann DH, Takahashi R, Misawa H & Cleveland DW (2008) Astrocytes as determinants of disease progression in inherited ALS. *Nat Neurosci* 11: 251–253
Yan X, Kuster D, Mohanty P, Nijssen J, Pombo-García K, Morato JG, Rizuan A, Franzmann TM, Sergeeva A, Ly AM, *et al* (2025) Intra-condensate demixing of TDP-43 inside stress granules generates pathological aggregates. *Cell* 188: 4123-4140.e18
Yang C, Wang H, Qiao T, Yang B, Aliaga L, Qiu L, Tan W, Salameh J, McKenna-Yasek DM, Smith T, *et al* (2014) Partial loss of TDP-43 function causes phenotypes of amyotrophic lateral sclerosis. *Proceedings of the National Academy of Sciences* 111: E1121–E1129
Zanini G, Selleri V, Nasi M, De Gaetano A, Martinelli I, Gianferrari G, Lofaro FD, Boraldi F, Mandrioli J & Pinti M (2022) Mitochondrial and Endoplasmic Reticulum Alterations in a Case of Amyotrophic Lateral Sclerosis Caused by TDP-43 A382T Mutation. *Int J Mol Sci* 23: 11881
Zhang Q-J, Lin J, Wang Y-L, Chen L, Ding Y, Zheng F-Z, Song H-H, Lv A-W, Li Y-Y, Guo Q-F, *et al* (2024) Detection of pTDP-43 via routine muscle biopsy: A promising diagnostic biomarker for amyotrophic lateral sclerosis. *Brain Pathology* 34: e13261
Zhou T, Ahmad TK, Gozda K, Truong J, Kong J & Namaka M (2017) Implications of white matter damage in amyotrophic lateral sclerosis. *Mol Med Rep* 16: 4379–4392